Article

Allosteric modulation of GPCR-induced β-arrestin trafficking and signaling by a synthetic intrabody

Mithu Baidya[1,7], Madhu Chaturvedi[1,7], Hemlata Dwivedi-Agnihotri[1,7], Ashutosh Ranjan[1], Dominic Devost [2], Yoon Namkung [3], Tomasz Maciej Stepniewski[4,5], Shubhi Pandey[1], Minakshi Baruah[1], Bhanupriya Panigrahi[1], Parishmita Sarma[1], Manish K. Yadav[1], Jagannath Maharana[1], Ramanuj Banerjee[1], Kouki Kawakami[6], Asuka Inoue[6], Jana Selent[4], Stéphane A. Laporte [2,3], Terence E. Hébert[2] & Arun K. Shukla [1]✉

Agonist-induced phosphorylation of G protein-coupled receptors (GPCRs) is a primary determinant of β-arrestin (βarr) recruitment and trafficking. For several GPCRs such as the vasopressin receptor subtype 2 (V_2R), agonist-stimulation first drives the translocation of βarrs to the plasma membrane, followed by endosomal trafficking, which is generally considered to be orchestrated by multiple phosphorylation sites. We have previously shown that mutation of a single phosphorylation site in the V_2R (i.e., V_2R^{T360A}) results in near-complete loss of βarr translocation to endosomes despite robust recruitment to the plasma membrane, and compromised ERK1/2 activation. Here, we discover that a synthetic intrabody (Ib30), which selectively recognizes activated βarr1, efficiently rescues the endosomal trafficking of βarr1 and ERK1/2 activation for V_2R^{T360A}. Molecular dynamics simulations reveal that Ib30 enriches active-like βarr1 conformation with respect to the inter-domain rotation, and cellular assays demonstrate that it also enhances βarr1-$β_2$-adaptin interaction. Our data provide an experimental framework to positively modulate the receptor-transducer-effector axis for GPCRs using intrabodies, which can be potentially integrated in the paradigm of GPCR-targeted drug discovery.

G protein-coupled receptors (GPCRs) recognize a broad spectrum of ligands and play critical roles in nearly every aspect of human physiology[1,2], and these receptors continue to be a major class of targets for novel drug discovery[3]. The spatio-temporal aspects of GPCR signaling are tightly regulated by multifunctional proteins, β-arrestins (βarrs)[4,5], and agonist-induced phosphorylation of GPCRs is a key determinant of βarr interaction and their ensuing functional outcomes[6,7]. While some GPCRs interact transiently with βarrs at the plasma membrane followed by rapid dissociation, others display a prolonged interaction resulting in endosomal trafficking of receptor-

[1]Department of Biological Sciences and Bioengineering, Indian Institute of Technology, Kanpur 208016, India. [2]Department of Pharmacology and Therapeutics, McGill University, Montréal, QC H3G 1Y6, Canada. [3]Department of Medicine, McGill University Health Center, McGill University, Montréal, QC H4A 3J1, Canada. [4]Research Program on Biomedical Informatics (GRIB), Department of Experimental and Health Sciences of Pompeu Fabra University (UPF)-Hospital del Mar Medical Research Institute (IMIM), 08003 Barcelona, Spain. [5]Faculty of Chemistry, Biological and Chemical Research Centre, University of Warsaw, Warsaw, Poland. [6]Graduate School of Pharmaceutical Sciences, Tohoku University, Sendai, Miyagi 980-8578, Japan. [7]These authors contributed equally: Mithu Baidya, Madhu Chaturvedi, Hemlata Dwivedi-Agnihotri. ✉e-mail: arshukla@iitk.ac.in

βarr complexes[8]. These two patterns of βarr interaction and trafficking have been used to categorize corresponding receptors as class A or class B GPCRs, respectively[8]. Interestingly, distinct phosphorylation patterns on GPCRs have been linked to different βarr conformations, which in turn determine the resulting functional responses[9–11]. While cumulative phosphorylation on GPCRs is typically believed to determine the affinity of βarr interaction, emerging evidence now suggests that spatial positioning of even single phosphorylation sites may provide a decisive contribution to βarr recruitment and subsequent functional outcomes[10–12].

We previously reported that mutation of a single phosphorylation site in the vasopressin receptor subtype 2 (V_2R) at Thr^{360} in the carboxyl-terminus (i.e., V_2R^{T360A}) dramatically altered βarr trafficking patterns[10]. V_2R is a class B receptor in terms of βarr interaction and trafficking where agonist stimulation first results in membrane recruitment of βarrs, followed by endosomal co-localization[8]. Interestingly, upon agonist-stimulation of V_2R^{T360A}, βarrs efficiently translocate to the plasma membrane, but do not traffic to endosomal compartments, unlike the wild-type receptor even after prolonged agonist-exposure (Fig. 1a)[10]. V_2R^{T360A} also exhibits reduced levels of ERK1/2 activation compared to the wild-type receptor without any measurable effect on G protein-coupling as assessed by measuring cAMP production[10]. This mutation leads to the disruption of a salt-bridge with Lys^{294} in βarr1 and consequently reduces the fraction of active βarr1 conformation as assessed using molecular dynamics simulation[10]. While V_2R^{T360A} exhibits a dramatic alteration in βarr1 trafficking pattern, the other phospho-site mutants behave either like wild-type (e.g. V_2R^{S357A} and V_2R^{T359A}) or exhibit a near-complete loss of βarr1 translocation to the membrane (e.g. $V_2R^{S362A/S363A/S364A}$)[10]. This prompted us to probe the conformation of βarr1 in the context of this receptor mutant (V_2R^{T360A}) and compare it with the wild-type V_2R, using a previously described intrabody30 (Ib30) based sensor[13].

Here, we show that Ib30 robustly recognizes βarr1 recruited to the plasma membrane upon agonist-stimulation of V_2R^{T360A}, and it rescues endosomal localization of βarr1 and ERK1/2 activation for V_2R^{T360A} to the levels of the wild-type receptor. We also discover that Ib30 enriches an active-like conformational population of βarr1 and also enhances the interaction of βarr1 with β2-adaptin. These findings establish the capability of Ib30 to allosterically modulate βarr1 trafficking and activation for V_2R^{T360A}, and potentially open a paradigm to modulate GPCR signaling using designer allosteric modulators.

Results
βarr1 conformation induced by V_2Rpp^{T360} phospho-peptides
Synthetic phospho-peptides corresponding to the carboxyl-terminus of V_2R have previously been used to activate βarrs in-vitro and probe the activation-induced conformational changes[14,15]. Therefore, we first synthesized two phospho-peptides corresponding to V_2R^{T360} mutation to probe whether the absence of Thr^{360} phosphorylation influences βarr1 conformation. These two phospho-peptides, referred to as V_2Rpp^{T360-1} and V_2Rpp^{T360-2}, contain a non-phosphorylated threonine (T) or alanine (A) at position 360, respectively, while the rest of the sequence and phosphorylation patterns are identical to V_2Rpp (referred to as V_2Rpp^{WT}) (Fig. 1b). We used a previously described limited trypsin proteolysis assay[15] to compare βarr1 conformation induced by V_2Rpp^{T360} phospho-peptides with that of V_2Rpp^{WT}. We observed that the activation of βarr1 by V_2Rpp^{WT} resulted in an accelerated cleavage of the 48 kDa band (Gly^{-8}-Arg^{418}), protection of 47 kDa and 45 kDa bands (Leu^1-Arg^{418} and Leu^1-Arg^{393}, respectively) and appearance of a 21 kDa band (Leu^1-Arg^{188}) (Fig. 1c, d, Supplementary Fig. 1a, b) as reported previously[15]. Interestingly, V_2Rpp^{T360} phospho-peptides also induced a proteolysis pattern qualitatively similar to that observed for V_2Rpp^{WT}, although there were noticeable differences such as relatively slower proteolysis of the 48 kDa band and a weaker intensity of the 21 kDa band (Fig. 1c, d and Supplementary Fig. 1a, b). The difference in

the intensity of 48 kDa and 47 kDa bands are visualized better at 1:50 ratio of trypsin:βarr1 (Fig. 1c, right half), while the difference in the 32 kDa and 21kda bands are visualized better at 1:25 ratio (Fig. 1c, left half). This observation indicates that V_2R^{T360} phospho-peptides are capable of binding βarr1; however, they do not induce active βarr1 conformation as stabilized by V_2R^{WT} but instead appear to promote an intermediate state between the basal and active-conformations.
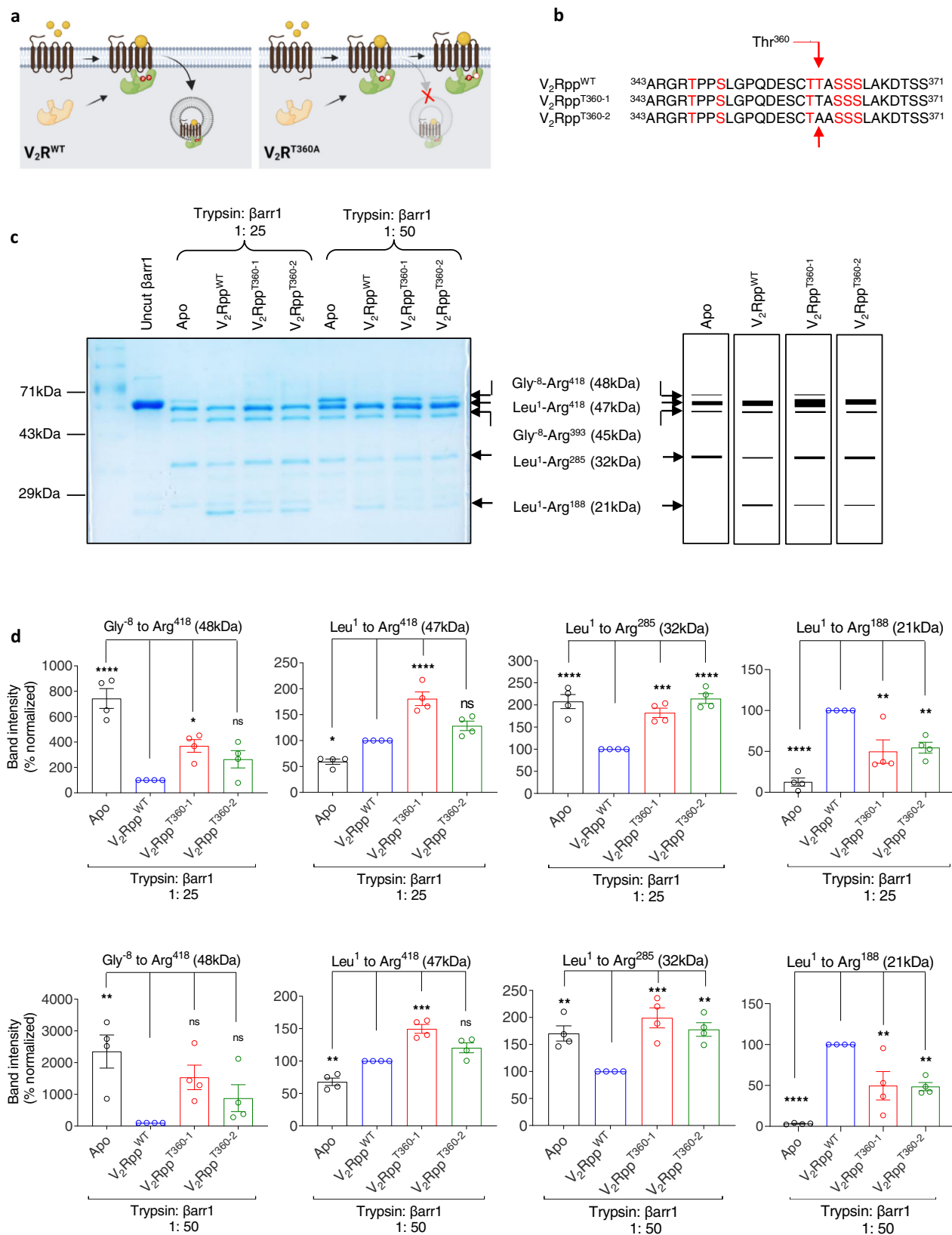
Fab30/ScFv30 sensors recognize V_2Rpp^{T360}-βarr1 complexes
As an additional readout of βarr1 conformation induced by V_2Rpp^{WT} vs. V_2Rpp^{T360} phospho-peptides, we measured the ability of antibody fragments referred to as Fab30/ScFv30 to recognize V_2Rpp-βarr1 complexes using co-immunoprecipitation (co-IP). Fab30 and ScFv30 are known to selectively recognize βarr1 conformation induced by V_2Rpp^{WT}, and thus, they have been used previously as conformational biosensors to monitor βarr activation in vitro[13,16]. We observed that Fab30/ScFv30 robustly interacted with the $V_2Rpp^{T360-1/2}$-βarr1 complexes, albeit at lower levels than V_2Rpp^{WT} (Fig. 2a–d). We carried out co-IP in the presence of either 10-fold or 50-fold molar excess of the phospho-peptides compared to βarr1, but the reactivity patterns of Fab30/ScFv30 did not change significantly (Fig. 2a–d). Similar to the limited proteolysis data presented in Fig. 1, these data also suggest that V_2Rpp^{T360} phospho-peptides induce a conformation in βarr1, which is qualitatively similar to that of V_2Rpp^{WT}, but not identical. However, we cannot rule out the possibility that the binding affinities of Fab30 and ScFv30 for βarr1-$V_2Rpp^{T360-1/2}$ complexes are relatively lower compared to βarr1-V_2Rpp^{WT} complex, which requires additional experimentation.

Considering the patterns of limited proteolysis and Fab30/ScFv30 reactivity induced by these phospho-peptides, we next carried out limited proteolysis assays in the presence of ScFv30 (Fig. 2e, f, Supplementary Fig. 2). We observed that the 47 kDa band (Leu^1-Arg^{418}) was significantly protected in presence of ScFv30, and the bands at 32 kDa and 21 kDa (Leu^1-Arg^{285} and Leu^1-Arg^{188}, respectively) did not appear (Fig. 2e, f, Supplementary Fig. 2). Interestingly, the proteolysis patterns observed in presence of ScFv30 were nearly-identical for V_2Rpp^{WT} and $V_2Rpp^{T360-1/2}$ phospho-peptides, although an additional band at ~30 kDa was observed only with V_2Rpp^{WT} (Fig. 2e, f). The converging proteolysis patterns of βarr1 observed in the presence of ScFv30 for the wild-type and mutant peptides suggest that ScFv30 might be promoting the transition of V_2Rpp^{T360}-bound βarr1 conformation towards the active-like state.

Structural insights into βarr1 conformation induced by V_2Rpp^{WT} and V_2Rpp^{T360}
Taking a lead from the limited proteolysis assays, we next analyzed the crystal structures of βarr1 in basal, V_2Rpp^{WT}-, and V_2Rpp^{T360}-bound states to gain further insights into βarr1 conformation. As the distal carboxyl-terminus of βarr1 is not resolved in these structures, we focused primarily on Arg^{285} and Arg^{188}, which are the trypsin cleavage sites yielding the 32 kDa (Leu^1-Arg^{285}) and 21 kDa (Leu^1-Arg^{188}) bands, respectively. Both of these residues exhibit a reorientation of their side chains between basal and phospho-peptide-bound conformations (Fig. 3a). The network of interactions involving Arg^{285} and Arg^{188} are also mostly maintained between basal and peptide-bound conformations although there are some differences as well (Fig. 3a). Further analysis of the local interaction networks of Arg^{188} and Arg^{285} using CONTACT/ACT program within the CCP4 suite[17], which analyzes all possible contacts/interactions and distances between residues in protein structures, including water molecules within a specified distance, also converges to the same observation as evident from the crystal structures (Supplementary Fig. 3). We also carried out molecular dynamics (MD) simulation studies using the crystal structures of βarr1 as templates to probe the conformational ensemble sampled by Arg^{188} and Arg^{285}, and observed that they explore similar conformational space in the wild-type and mutant phospho-peptide-bound

a

b

Thr^{360}

V$_2$Rpp^{WT} ^{343}ARGRTPPSLGPQDESCTTASSSLAKDTSS^{371}
V$_2$Rpp^{T360-1} ^{343}ARGRTPPSLGPQDESCTTASSSLAKDTSS^{371}
V$_2$Rpp^{T360-2} ^{343}ARGRTPPSLGPQDESCTAASSSLAKDTSS^{371}

c

Gly^{-8}-Arg^{418} (48kDa)
Leu^1-Arg^{418} (47kDa)
Gly^{-8}-Arg^{393} (45kDa)
Leu^1-Arg^{285} (32kDa)
Leu^1-Arg^{188} (21kDa)

d

Gly^{-8} to Arg^{418} (48kDa)

Leu^1 to Arg^{418} (47kDa)

Leu^1 to Arg^{285} (32kDa)

Leu^1 to Arg^{188} (21kDa)

Trypsin: βarr1 1:25

Gly^{-8} to Arg^{418} (48kDa)

Leu^1 to Arg^{418} (47kDa)

Leu^1 to Arg^{285} (32kDa)

Leu^1 to Arg^{188} (21kDa)

Trypsin: βarr1 1:50

states (Fig. 3b). Taken together, these structural insights provide a plausible explanation for the proteolysis patterns obtained for V$_2$Rpp^{WT} vs. V$_2$Rpp^{T360}, and support the hypothesis that V$_2$Rpp^{T360} induces an intermediate conformation in βarr1 compared to apo- and V$_2$R^{WT}-bound states that may be further influenced by the binding of Fab30.

Agonist-induced βarr1 recruitment to V$_2$R^{WT} and V$_2$R^{T360A}
The experiments presented so far were carried out in-vitro using isolated phospho-peptides, and therefore, we next set out to measure the relative recruitment of βarr1 and the reactivity of Ib30, an intrabody derived from Fab30 that reports βarr1 activation and trafficking[11,13], for the wild-type V$_2$R (V$_2$R^{WT}) and the mutant receptor (V$_2$R^{T360A}). We first

Fig. 1 | V$_2$Rpp^{WT} and V$_2$Rpp^{T360} impart different conformations on βarr1.
a Schematic representation of the inability of V$_2$R^{T360A} mutant to promote endo-somal trafficking of βarr1 as published previously. **b** Amino acid sequences of the V$_2$R^{WT} and Thr^{360} mutant phospho-peptides (V$_2$Rpp^{T360-1} and V$_2$Rpp^{T360-2}) were used in this study. Phosphorylated residues (serine, S; threonine, T) are highlighted in red, and the position 360 is indicated by an arrow. V$_2$Rpp^{T360-1} and V$_2$Rpp^{T360-2} contain a non-phosphorylated threonine and an alanine at position 360, respectively. **c** Limited trypsin proteolysis of βarr1 (5 min) in the absence or presence of indicated phospho-peptides at two different trypsin: βarr1 ratio followed by visualization of the bands on SDS-PAGE. A representative gel from four independent experiments (left panel) and a schematic of the proteolysis pattern corresponding to 1: 25 ratio of trypsin:βarr1 (right panel) is shown here. **d** Densitometry-based quantification (mean ± SEM) of indicated bands from four independent experiments, normalized

with respect to V$_2$Rpp^{WT} condition (treated as 100%) (One-way ANOVA, Dunnett's multiple comparisons test). The exact p values are as follows: Gly^{-8} to Arg^{418} (48 kDa) band (1: 25)- Apo ($p < 0.0001$), V$_2$R^{T360-1} ($p = 0.0159$), V$_2$R^{T360-2} ($p = 0.1539$); Gly^{-8} to Arg^{418} (48 kDa) band (1: 50)- Apo ($p = 0.0039$), V$_2$R^{T360-1} ($p = 0.0566$), V$_2$R^{T360-2} ($p = 0.385$); Leu^1 to Arg^{418} (47 kDa) band (1: 25)-Apo ($p = 0.0132$), V$_2$R^{T360-1} ($p < 0.0001$), V$_2$R^{T360-2} ($p = 0.0844$); Leu^1 to Arg^{418} (47 kDa) band (1: 50)-Apo ($p < 0.0024$), V$_2$R^{T360-1} ($p = 0.0001$), V$_2$R^{T360-2} ($p = 0.059$); Leul^1 to Arg$_2^{85}$ (32 kDa) band (1: 25)-Apo($p < 0.0001$), V$_2$R^{T360-1} ($p = 0.0006$), V$_2$R^{T360-2} ($p < 0.0001$); Leul^1 to Arg^{285} (32 kDa) band (1: 50)-Apo($p = 0.0072$), V$_2$R^{T360-1} ($p = 0.0005$), V$_2$R^{T360-2} ($p = 0.0036$); Leul^1 to Arg^{188} (21 kDa) band (1: 25)-Apo ($p < 0.0001$), V$_2$R^{T360-1} ($p = 0.0028$), V$_2$R^{T360-2} ($p = 0.0057$); Leul^1 to Arg^{188} (21 kDa) band (1: 50)-Apo($p < 0.0001$), V$_2$R^{T360-1} ($p = 0.005^1$), V$_2$R^{T360-2} ($p = 0.0044$). Source data are provided as a Source Data file (*$p < 0.05$, **$p < 0.01$, ***$p < 0.001$, ****$p < 0.0001$, ns = non-significant).

used a NanoBiT assay that measures the direct binding of the receptor and βarr1 and, therefore, reports cumulative interaction resulting from both the cell surface and internalized pools (Fig. 4a). We observed that the total βarr1 recruitment to V$_2$R^{T360A} mutant was significantly atte-nuated compared to the V$_2$R^{WT} (Fig. 4b), and this is in excellent agreement with our previous study using the Tango assay[10]. Next, we compared the surface recruitment of βarr1 to the wild-type and mutant receptor using a NanoBiT assay where the LgBiT component is teth-ered to the plasma membrane through CAAX sequence while βarr1 is tagged with SmBiT (Fig. 4c). Here, we observed a near-identical pattern of βarr1 recruitment for the V$_2$R^{WT} and V$_2$R^{T360A} suggesting that endo-somal trafficking but not surface translocation is compromised by the Thr^{360}Ala mutation in the V$_2$R (Fig. 4d). These findings, therefore, set the stage for testing whether Ib30 can recognize the βarr1 conforma-tion induced by V$_2$R^{T360A} and influence its endosomal trafficking. In these experiments, surface expression of the V$_2$R^{WT} and V$_2$R^{T360A} were comparable as measured using whole-cell ELISA assay (Supplementary Fig. 4a, b).

**Intrabody30 rescues endosomal trafficking of βarr1 for V$_2$R^{T360A}**
We first co-expressed SmBiT-βarr1 and LgBiT-Ib30 constructs with V$_2$R^{WT} and V$_2$R^{T360A} and measured agonist-induced changes in lumi-nescence signal as a readout of βarr1-Ib30 interaction and conforma-tional recognition of βarr1 by Ib30 (Fig. 5a). As Ib30 reactivity is expected to follow cumulative βarr1 recruitment upon receptor acti-vation, we anticipated a relatively lower response for V$_2$R^{T360A} com-pared to V$_2$R^{WT} considering their total βarr1 recruitment patterns as presented in Fig. 4b. Surprisingly, however, we observed nearly-identical response for Ib30 reactivity upon agonist-stimulation for both, V$_2$R^{WT} and V$_2$R^{T360A} (Fig. 5b). This finding not only suggests that the conformation of βarr1 induced by V$_2$R^{T360A} in the cellular context is recognizable by the Ib30 sensor, but also that Ib30 might be rescuing endosomal trafficking of βarr1 and thereby, bringing the overall recruitment to the wild-type level. We tested this hypothesis by mea-suring the overall βarr1 recruitment for V$_2$R^{WT} and V$_2$R^{T360A} in a NanoBiT assay in presence of either a control intrabody (Ib-CTL) or Ib30. In fact, we observed that overall βarr1 recruitment for V$_2$R^{T360A} becomes nearly-identical to that of V$_2$R^{WT} upon co-expression of Ib30 (Supple-mentary Fig. 5). In these NanoBiT experiments, the V$_2$R^{WT} and V$_2$R^{T360A} were expressed at comparable levels as measured in terms of their surface expression (Supplementary Fig. 4c, d). We also measured agonist-induced G protein-coupling for the V$_2$R^{T360A} in the presence of Ib-CTL and Ib-30 but did not observe any significant difference, similar to the V$_2$R^{WT} (Supplementary Fig. 6a, b), suggesting the specificity of Ib30 for receptor-βarr interaction without a measurable effect on G proteincoupling.

In order to directly visualize the ability of Ib30 to recognize βarr1 upon recruitment to V$_2$R^{T360A}, we co-expressed Ib30-mYFP construct together with βarr1-mCherry in HEK-293 cells expressing V$_2$R^{T360A}, and monitored localization of βarr1 and Ib30 by confocal microscopy. Ib30

translocated to the plasma membrane upon agonist-stimulation, similar to βarr1, and exhibited robust colocalization with βarr1 (Fig. 5c, d). Interestingly, we also observed that upon prolonged agonist expo-sure (>15 min), both βarr1 and Ib30 were translocated to endosomal vesicles and robustly co-localized (Fig. 5c, d). This observation further strengthens the hypothesis that Ib30 may potentially be rescuing endosomal trafficking of βarr1 for V$_2$R^{T360A} as hinted in the NanoBiT-based Ib30 recognition assay (Fig. 5a, b) and overall βarr1 recruitment assay for V$_2$R^{T360A} (Supplementary Fig. 5). To further corroborate these findings and directly establish the allosteric potentiation of endosomal trafficking of βarr1 by Ib30, we used three different approaches. First, we co-expressed a βarr1-mYFP construct in HEK-293 cells together with either V$_2$R^{WT} or V$_2$R^{T360A} in the presence or absence of HA-tagged Ib30. We monitored the localization of βarr1 in these cells upon agonist-simulation using confocal microscopy and scored the localization pattern of βarr1 in terms of plasma membrane vs. internalized vesicles. We manually scored more than 500 cells for each condition and plotted the data as % normalized (i.e. % of total cells displaying mem-brane vs. punctate localization of βarr1). In line with data presented in Fig. 5c, d, we observed that the presence of Ib30 indeed promoted endosomal trafficking of βarr1 for V$_2$R^{T360A} (Fig. 5e, f) while βarr1 remained localized primarily at the plasma membrane even after prolonged agonist-exposure in the absence of Ib30, as reported previously[10].

Next, we used an intermolecular bystander BRET assay to monitor the endosomal localization of βarr1 quantitatively by using βarr1-R-Luc and GFP-FYVE constructs, described previously (Fig. 6a)[18]. As shown in Fig. 6b, we observed a very low level of agonist-induced BRET for V$_2$R^{T360A} in the presence of control intra-body (Ib-CTL), while V$_2$R^{WT} exhibited a robust response as expected. Interestingly, however, co-expression of Ib30 rescued the BRET sig-nal (i.e., endosomal trafficking of βarr1) to almost the same level as V$_2$R^{WT} (Fig. 6b, c). We also observed an enhanced E$_{max}$ in BRET assay for V$_2$R^{WT} in the presence of Ib30, compared to Ib-CTL, although basal BRET was also higher and therefore, the change in BRET signal is significantly more pronounced for the V$_2$R^{T360A} (Fig. 6c). Finally, we also carried out a similar experiment using the NanoBiT assay that measures endosomal trafficking of βarr1 based on similar principles as in BRET assay described above (Fig. 6d). We observed analogous potentiation of endosomal localization of βarr1 by Ib30 for V$_2$R^{T360A} as in BRET assay while there was no significant change for V$_2$R^{WT} (Fig. 6e, f). In these experiments, the surface expression of the V$_2$R^{WT} and V$_2$R^{T360A} were maintained at comparable levels to ensure that the observed differences did not arise from a difference in the expres-sion level of the wild-type and mutant receptors (Supplementary Fig. 4e). Taken together with the confocal microscopy observations, these data establish that Ib30 recognizes V$_2$R^{T360A}-bound βarr1 con-formation and allosterically potentiates its trafficking to endosomal vesicles and thereby, rescues the trafficking pattern of βarr1 making it similar to the wild-type receptor.
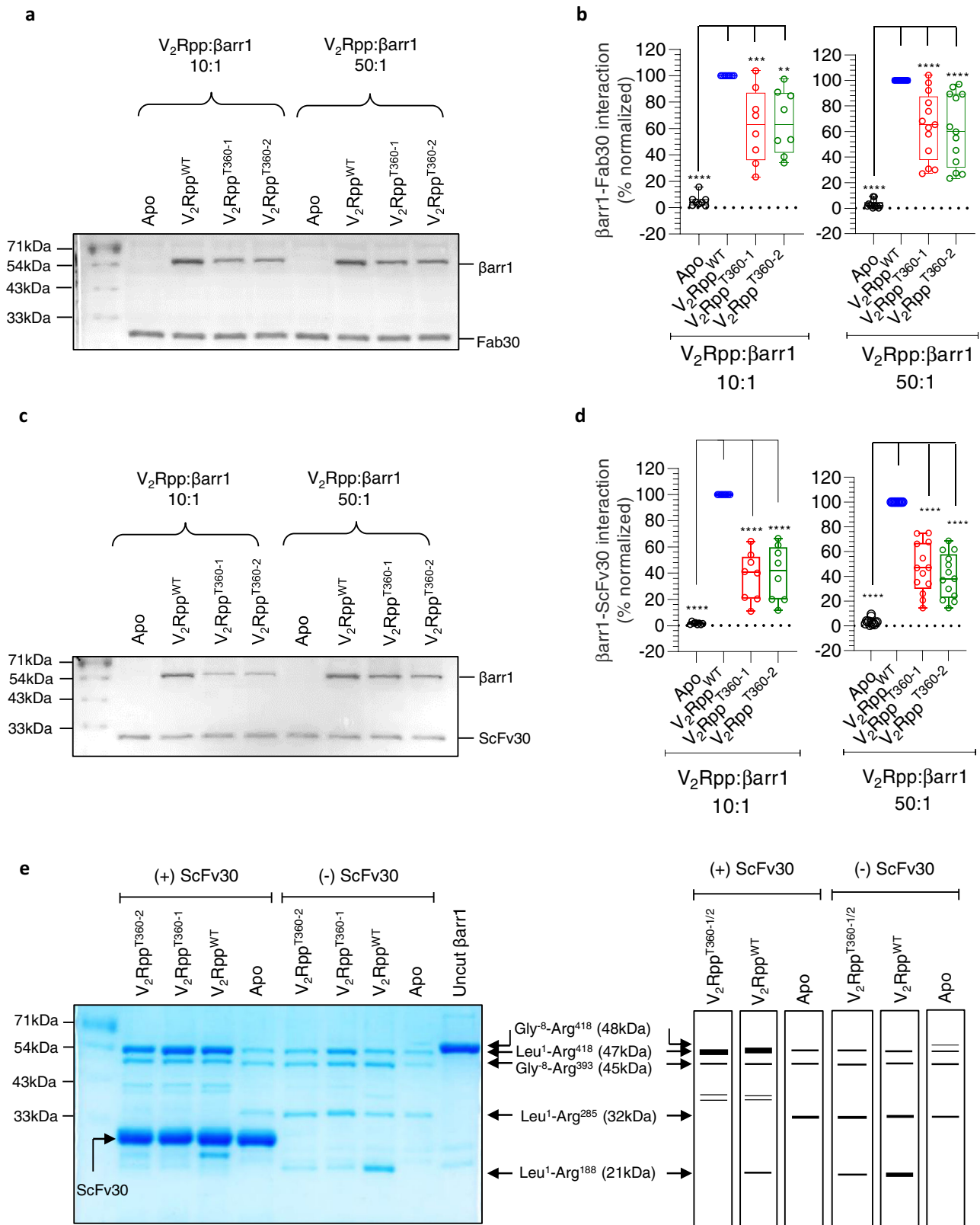
Intrabody30 rescues agonist-induced ERK1/2 activation for V₂R^T360A

We have previously reported that agonist-induced ERK1/2 MAP kinase activation is significantly attenuated for V_2R^{T360A} compared to the wild-type receptor[10]. Considering the potentiating effect of Ib30 on βarr1 trafficking, and previous studies linking endosomal pool of βarrs with ERK1/2 MAP kinase activation for GPCRs[19], we next measured the effect of Ib30 on agonist-induced ERK1/2 phosphorylation for the V_2R^{WT} and V_2R^{T360A}. Expectedly, Ib30 did not have a significant effect on ERK1/2 activation for the V_2R^{WT}, however, it robustly enhanced the level of phosphorylated ERK1/2 upon agonist-stimulation for V_2R^{T360A}, to the levels of the V_2R^{WT} (Fig. 7a, b). The surface expression of the wild-type

and mutant receptors were at comparable levels in these experiments (Supplementary Fig. 4f). Taken together with the endocytosis data, these findings demonstrate an allosteric effect of Ib30 to positively modulate βarr-mediated functional responses for the V_2R^{T360A} mutant in the cellular context.

Structural insights into the allosteric effect of Fab30 on βarr1 conformation

The positive allosteric effect of Ib30 on endosomal trafficking of βarr1 and ERK1/2 activation for V_2R^{T360A} prompted us to probe the potential structural mechanism for this phenomenon at the level of phospho-peptide binding and βarr1 conformation. Therefore, we first analyzed the crystal structures of V_2Rpp^{WT}-βarr1 (PDB: 4JQI) and V_2Rpp^{T360-1}-βarr1 (PDB: 7DFA), determined previously. Interestingly, a segment of the V_2Rpp^{T360-1} containing residues Pro353 to Thr360 showed a marked repositioning compared to the V_2Rpp^{WT} binding pose (Fig. 8a). In the V_2Rpp^{WT}-βarr1 crystal structure, pThr360 engages Lys294, Lys11 and Arg25 in βarr1 through ionic interactions, which is expectedly absent in case of V_2Rpp^{T360} mutation. Of these, Lys294 in the lariat loop and Lys11 in the β-strand I of βarr1 are particularly noteworthy as they constitute a key part of the polar core and phosphate sensor, respectively[7]. These interactions are critical in the process of βarr1 activation upon binding of phosphorylated carboxyl-terminus of GPCRs. Interestingly, pThr359 in V_2Rpp^{T360} phospho-peptide engages with Lys11 but not with Lys294 or Arg25. This interesting structural rearrangement may, in part explain an intermediate active-like conformation induced by V_2Rpp^{T360} phospho-peptides as observed in limited proteolysis and ScFv30 co-IP assay.

Next, we used molecular dynamics (MD) simulation on V_2Rpp^{WT}- and V_2Rpp^{T360A}-bound βarr1. We have previously reported that Thr360Ala mutation resulted in a significant shift in the population of βarr1 towards inactive-like conformation compared to the V_2Rpp^{WT} as measured in terms of the inter-domain rotation angle[10]. We also found that the Thr360Ala mutation leads to the disruption of a salt-bridge with Lys294 in the lariat loop of βarr1, which links the N- to the C-domain via the phospho-peptide, and removing this inter-domain connector may reverse the inter-domain rotation leading to the transition of βarr1 towards inactive conformation[10]. Now, in this study, we first reproduced this behavior for the V_2Rpp^{T360A} mutant, demonstrating that introducing the Thr360Ala mutation in the V_2Rpp-βarr1 complex leads to a dramatic shift towards inactive-like conformations with an inter-domain rotation angles <15° (i.e. V_2Rpp^{WT}: 24% vs. V_2Rpp^{T360A}: 63%) (Fig. 8b–d). Strikingly, simulations of the V_2Rpp^{T360A}-βarr1 complex in presence of Fab30 revealed that Fab30 binding significantly stabilizes the population of active-like βarr1 conformations (V_2Rpp^{T360A} + Fab30: 70% vs. V_2Rpp^{T360A}: 37%) (Fig. 8b–d). This interesting observation can be rationalized by the fact that Fab30 simultaneously binds to the N- and the C-domain of βarr1, which blocks the reversal of the inter-domain rotation towards inactive-like βarr1 conformations. This stabilizing contribution of Fab30 towards active-like βarr1 conformations may offer a plausible mechanism for the positive allosteric effect of

Ib30 observed on βarr1 trafficking to endosomes and agonist-induced ERK1/2 activation for the V_2R^{T360A}.

It is worth noting here that despite an accumulated simulation time of 10μs per system (i.e. 5 runs of 2 μs), our simulation set up does not allow for a converged sampling of βarr1 ensemble. However, the running averages of the inter-domain rotation angle show that βarr1 can transition between active- and inactive-like states in all three conditions (i.e. V_2Rpp^{WT}, V_2Rpp^{T360A}, and V_2Rpp^{T360A} + Fab30). This indicates that βarr1 explores a wide range of conformational landscape and that observed tendencies are not an artifact but rather describe an actual property of each system.

Intrabody30 enhances βarr1-β₂-adaptin interaction

Next, we set out to identify a potential functional correlate of Ib30-induced enrichment of active-like βarr1 conformation and to reveal the mechanism of Ib30-mediated endosomal targeting of βarr1. As the interaction of βarrs with β₂-adaptin is a prominent mechanism that drives GPCR endocytosis[5,20], we measured the effect of Ib30 on βarr1-β₂-adaptin interaction. We used the ear-domain of β₂-adaptin (592–951) tagged with GST at the N-terminus and assessed its interaction with βarr1 in the presence of lysate prepared from *Sf*9 cells expressing V_2R^{T360A}. The ear domain represents the C-terminal appendage of the β₂-adaptin subunit of the clathrin adaptor AP2 complex, and this region has been shown previously to interact with βarr1[21]. As presented in Fig. 9a, b, we observed a low but statistically significant interaction between βarr1 and β₂-adaptin in the presence of Ib-CTL. More interestingly, the presence of Ib30 enhanced this interaction several fold suggesting the ability of Ib30 to promote βarr1-β₂-adaptin interaction (Fig. 9a, b).

To further corroborate this interesting finding in cellular context, we next used a previously described BRET-based assay[22] to monitor agonist-induced interaction of βarr1 with β₂-adaptin in the presence of either Ib-CTL or Ib30 for V_2R^{WT} and V_2R^{T360A} (Fig. 9c). There was a robust interaction between βarr1 and β₂-adaptin for the V_2R^{WT} upon agonist-stimulation in the presence of Ib-CTL, while the response was significantly lower for the V_2R^{T360A}. This is in line with significantly attenuated endosomal trafficking of βarr1 for the V_2R^{T360A} compared to V_2R^{WT}. Interestingly, co-expression of Ib30 significantly enhanced βarr1-β₂-adaptin interaction for V_2R^{T360A}, bringing it to almost the same level as V_2R^{WT}. However, the basal BRET signal was also higher under Ib30 expression conditions compared to Ib-CTL, and it may reflect the propensity of Ib30 to enhance βarr1-β₂-adaptin interaction, even under the basal condition i.e. without receptor activation (Fig. 9d). To test this hypothesis, we carried out a titration experiment, where we expressed Ib30 at increasing levels and assessed βarr1-β₂-adaptin interaction in the BRET assay. As presented in Fig. 9e, increasing expression of Ib30 indeed enhanced BRET in a saturable manner suggesting the ability of Ib30 to promote basal interaction between βarr1 and β₂-adaptin. Taken together, these observations provide a mechanistic basis of Ib30-induced allosteric modulation of βarr1 trafficking pattern observed for V_2R^{T360A}.
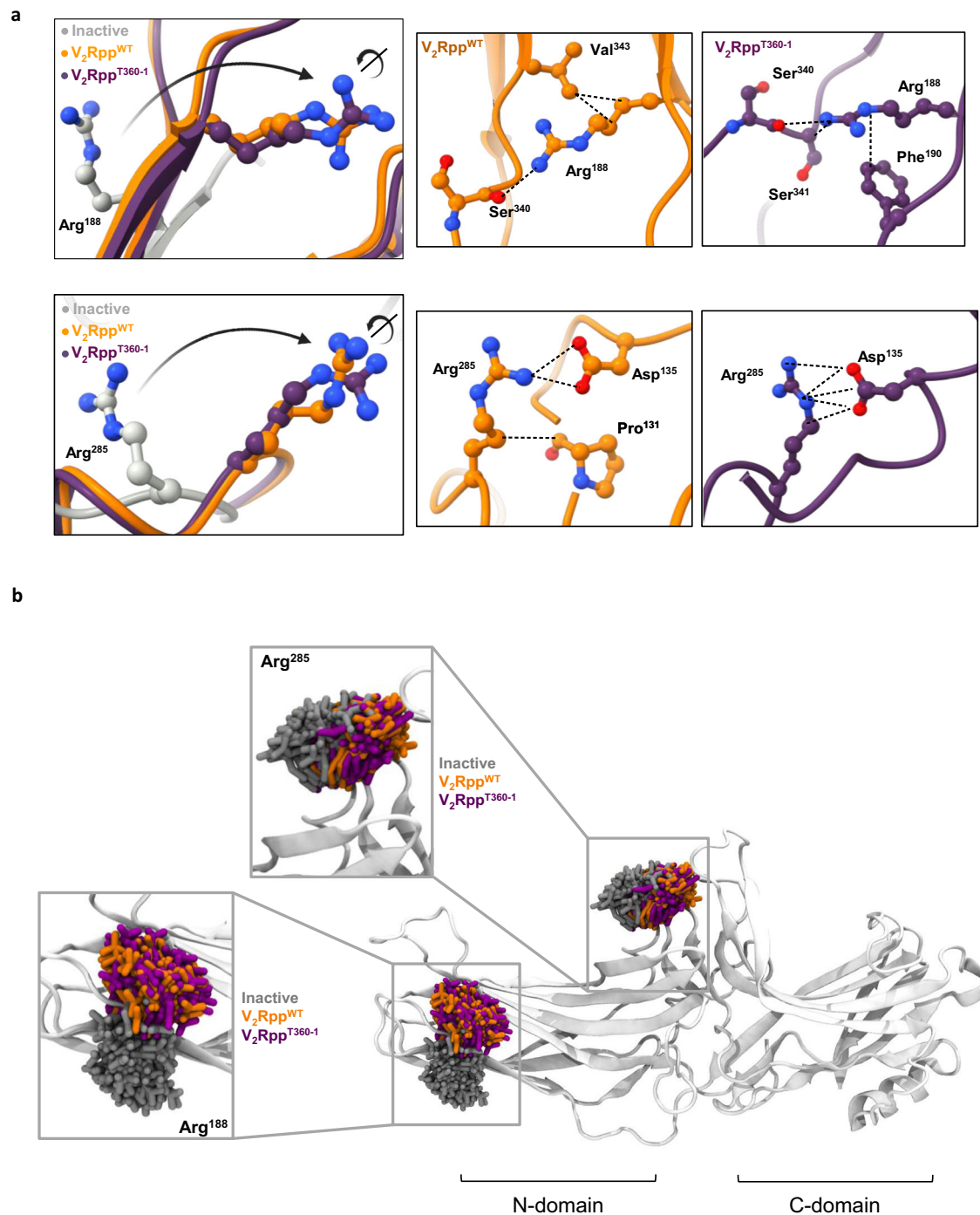
**Fig. 3 | Structural insights into binding of phospho-peptides to βarr1.**
a Structural snapshots comparing the relative orientation and local interaction networks of trypsin cleavage sites Arg[188] and Arg[285] in the crystal structures of βarr1 in basal (PDB: 1G4M, grey), V$_2$Rpp[WT]-bound (PDB: 4JQI, orange) and V$_2$Rpp[T360-1]- bound (PDB: 7DFA, violet) conformations. The dotted lines represent hydrogen bonds and polar interactions. **b** Molecular dynamics simulations based on the crystal structures confirm an overall similar conformational space sampled by Arg[188] and Arg[285], the two trypsin proteolysis sites which are protected by ScFv30.

Discussion

In this study, we demonstrate that a synthetic intrabody (Ib30) can allosterically modulate agonist-induced trafficking patterns of βarr1 for a vasopressin receptor subtype 2 mutant (V$_2$R[T360A]) lacking a key phosphorylation site in its carboxyl-terminus. Ib30 induces the transition of βarr1 trafficking pattern for V$_2$R[T360A] from class A to class B by enriching the fraction of active-like conformational population of βarr1, and allosterically enhancing βarr1-β$_2$-adaptin interaction. Moreover, Ib30 also rescues the attenuated ERK1/2 activation for V$_2$R[T360A] to levels induced by the wild-type receptor. A

previous study has demonstrated a critical role of βarr-β$_2$-adaptin interaction in βarr-mediated ERK1/2 activation for V$_2$R using a small molecule inhibitor of this interaction[22]. Therefore, an increase in βarr1-β$_2$-adaptin interaction in presence of Ib30 may provide a plausible mechanism for its ability to rescue agonist-induced ERK1/2 activation for V$_2$R[T360A]. However, additional mechanisms may also contribute to this intriguing observation, and it would be interesting to probe this further in subsequent studies. Although Ib30 appears to slightly enhance the endosomal trafficking of βarr1 for V$_2$R[WT] (Fig. 6b, c), an observation that is consistent with our
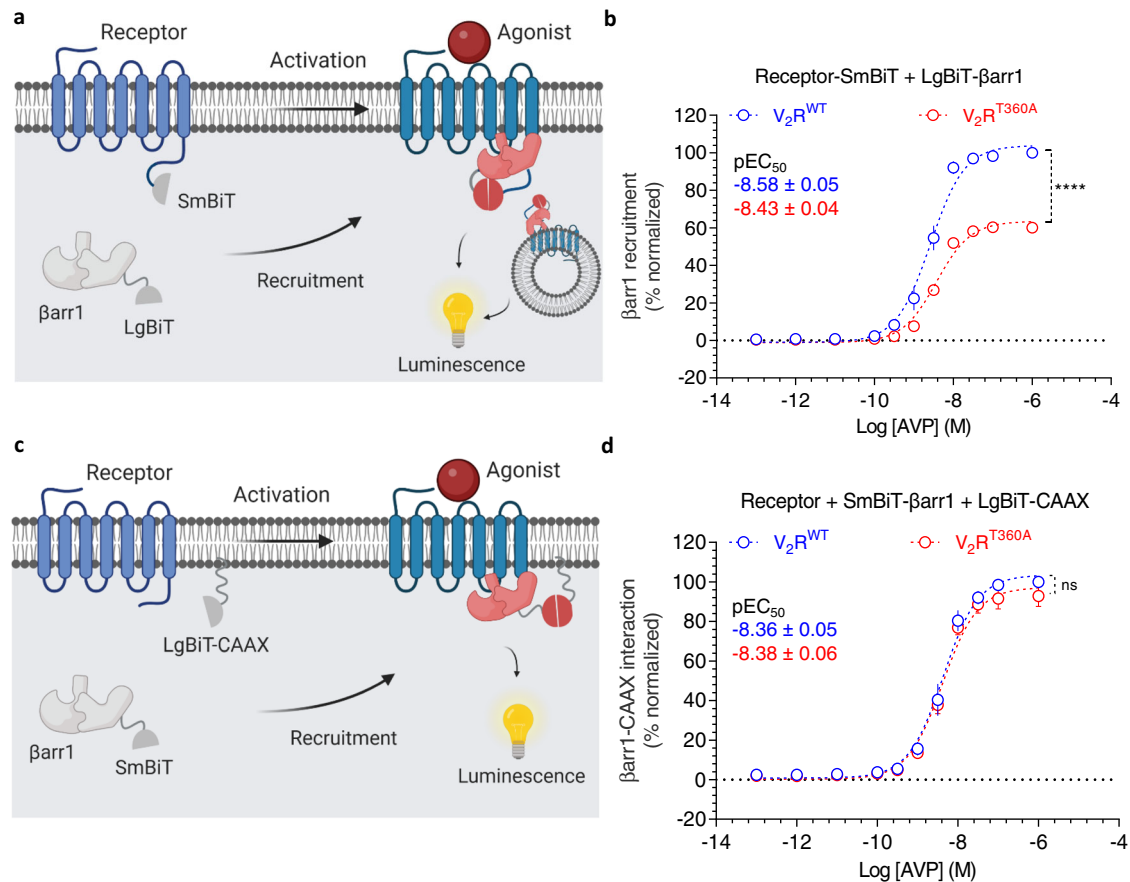
Fig. 4 | Agonist-induced βarr1 recruitment to V_2R^{WT} and V_2R^{T360A} mutant.
a Schematic representation of NanoBiT-based βarr1 recruitment assay. **b** HEK-293 cells expressing the indicated receptor and βarr1 constructs were stimulated with varying doses of AVP for 30 min followed by the measurement of luminescence (mean ± SEM; $n = 4$ independent experiments; normalized with luminescence signal for V_2R^{WT} at maximal ligand dose as 100%, Two-way ANOVA, Sidak's multiple comparisons test; ****$p < 0.0001$). **c** Schematic representation of NanoBiT-based assay for measuring βarr1 translocation to the cell surface. **d** HEK-293 cells expressing the indicated receptor and βarr1 constructs together with LgBiT-CAAX were stimulated with varying doses of AVP for 30 min followed by the measurement of luminescence (mean ± SEM; $n = 4$ independent experiments; normalized with luminescence signal for V_2R^{WT} at maximal ligand dose as 100%, Two-way ANOVA, Sidak's multiple comparison test; ns = non-significant). Source data are provided as a Source Data file.
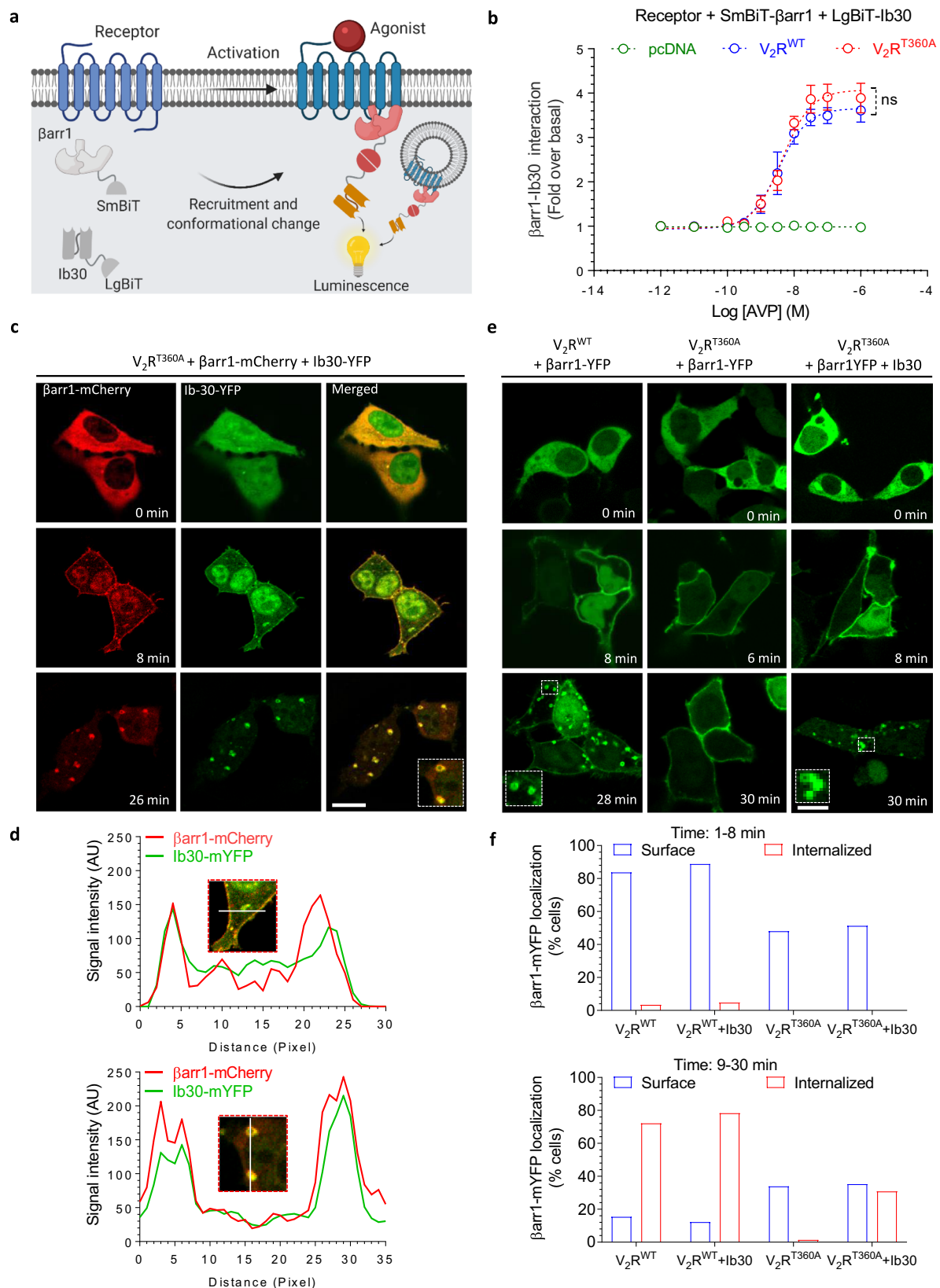
previous study[13], it does not significantly potentiate ERK1/2 activation (Fig. 7a, b). As we are measuring ERK1/2 activation after five minutes of agonist-stimulation, where the signal is typically maximal and saturated, Ib30-mediated potentiation of ERK1/2 response for V_2R^{WT}, if any, may not be apparent under these conditions.

While previous studies have used intrabodies as biosensors of GPCR activation[23], βarr trafficking[13], inhibitors of GPCR endocytosis[24] and Gβγ signaling[25], the current study provides an example of an intrabody-based approach to positively modulate βarr trafficking and functional outcomes. Considering the earlier studies reporting sustained cAMP generation from the internalized pool of V_2R, we anticipated an enhanced cAMP response for the V_2R^{T360A} in presence of Ib30 due to potentiation of βarr1 endosomal trafficking. However, we did not observe a significant difference in cAMP response between Ib-CTL vs. Ib30 conditions for V_2R^{T360A} (Supplementary Fig. 6a). While this may simply reflect an inherent limitation of the GloSensor assay due to robust signal amplification, it would be interesting to investigate this aspect further in future studies. For example, in case of wild-type V_2R, agonist-stimulation promotes co-localization of the receptor, βarr1 and Ib30 in endosomal vesicles[13] however, it is plausible that V_2R^{T360A} dissociates from βarr1 at the plasma membrane due to relatively lower affinity. This may lead to trafficking of βarr1, presumably stabilized in an active conformation by Ib30, to endosomal vesicles even in the absence of the receptor. Further investigation along these lines in future studies may also help clarify the underlying mechanism for the

lack of cAMP potentiation in case of V_2R^{T360A} despite enhanced endosomal trafficking of βarr1 in the presence of Ib30.

An elegant study has recently reported crystal structures of βarr1 in complex with several different phospho-peptides derived from the carboxyl-terminus of V_2R, including the V_2Rpp^{T360-1} [26]. While the binding affinities of βarr1 to V_2Rpp^{WT} and V_2Rpp^{T360-1} are comparable, V_2Rpp^{T360-1} exhibits a slightly altered binding mode compared to V_2Rpp^{WT} in these crystal structures[26]. Therefore, it is unlikely that distinct trafficking patterns of βarr1 for V_2R^{WT} vs. V_2R^{T360A} originate from an affinity difference, and it points towards a conformational mechanism underlying this phenomenon. This is indeed supported by our MD simulation studies, where Fab30 binding enriches active-like conformational populations in βarr1 with inter-domain rotation as a readout for the mutant phospho-peptide. GPCR-βarr interactions are typically thought to be biphasic and involve the phosphorylated carboxyl-terminus of the receptor and the cytoplasmic face of the activated transmembrane bundle[6,7,27–30]. Previous studies have visualized such partially-engaged and fully-engaged GPCR-βarr complexes and deciphered functional outcomes associated with these distinct conformations[28–30]. A recent study using NMR spectroscopy demonstrated that Fab30 binding to a partially-engaged GPCR-βarr complex facilitates additional conformational changes in βarr1 leading to a transition towards fully-activated conformation[31]. Our study now draws an interesting parallel with this recent NMR study by demonstrating that Ib30 allosterically facilitates the transition of a

a

Receptor — Activation — Agonist

βarr1

SmBiT — Recruitment and conformational change — Luminescence

Ib30 — LgBiT

b

Receptor + SmBiT-βarr1 + LgBiT-Ib30

pcDNA V_2R^{WT} V_2R^{T360A}

βarr1-Ib30 interaction (Fold over basal) vs Log [AVP] (M)

ns

c

V_2R^{T360A} + βarr1-mCherry + Ib30-YFP

βarr1-mCherry   Ib-30-YFP   Merged

0 min

8 min

26 min

e

V_2R^{WT} + βarr1-YFP V_2R^{T360A} + βarr1-YFP V_2R^{T360A} + βarr1YFP + Ib30

0 min

8 min / 6 min / 8 min

28 min / 30 min / 30 min

d

βarr1-mCherry
Ib30-mYFP

Signal intensity (AU) vs Distance (Pixel)

βarr1-mCherry
Ib30-mYFP

Signal intensity (AU) vs Distance (Pixel)

f

Time: 1-8 min

Surface   Internalized

βarr1-mYFP localization (% cells)

V_2R^{WT} V_2R^{WT}+Ib30 V_2R^{T360A} V_2R^{T360A}+Ib30

Time: 9-30 min

Surface   Internalized

βarr1-mYFP localization (% cells)

V_2R^{WT} V_2R^{WT}+Ib30 V_2R^{T360A} V_2R^{T360A}+Ib30

functionally-compromised βarr1 conformation to a fully-competent conformation for V_2R^{T360A}, and rescues downstream functional responses. It would be interesting to explore in future studies whether the effect of Ib30 observed here for V_2R^{T360A} is somehow linked to the transition between the partially- and fully-engaged βarr conformations in complex with the receptor.

The paradigm of βarr-AP2 interaction through $β_2$-adaptin in driving GPCR endocytosis via a clathrin-mediated pathway is mostly conserved across GPCRs[5]. Therefore, our study raises the possibility of Ib30 being a potentially generic positive modulator of βarr1 trafficking for other GPCRs as well, especially those exhibiting Class A pattern of βarr recruitment. Interestingly, we have already demonstrated the

Fig. 5 | Intrabody30 sensor efficiently recognizes βarr1 conformation induced by V_2R^{T360A}. a Schematic representation of NanoBiT-based assay to measure Ib30 reactivity to βarr1. **b** Recognition of βarr1 by Ib30 upon stimulation of V_2R^{WT} or V_2R^{T360A}. HEK-293 cells expressing the indicated receptor, βarr1 and Ib30 constructs were stimulated with varying doses of AVP for 30 min, followed by the measurement of luminescence (mean ± SEM; $n = 4$ independent experiments; normalized with luminescence signal for V_2R^{WT} at maximal ligand dose as 100%; Two-way ANOVA, Tukey's multiple comparisons test; ns = non-significant). **c** βarr1 and Ib30 are colocalized upon agonist-stimulation of V_2R^{T360A}. HEK-293 cells expressing V_2R^{T360A} together with βarr1-mCherry and Ib30-YFP were stimulated with AVP (100 nM) for indicated time-points followed by visualization using confocal microscopy. Micrographs are representative of three independent experiments (Scale bar 10 µm). Uncropped micrographs are available in the Source Data file.

d Line-scan analysis of the indicated regions from confocal micrographs confirms the colocalization of βarr1 and Ib30. **e** Expression of Ib30 drives endosomal localization of βarr1 for V_2R^{T360A}. HEK-293 cells expressing V_2R^{WT} or V_2R^{T360A} together with βarr1-YFP were stimulated with AVP (100 nM), and the localization of βarr1 was monitored using confocal microscopy (Scale bar 10 µm). **f** The effect of Ib30 on localization of βarr1 as assessed by manually scoring HEK-293 cells from multiple fields in three independent experiments. Captured confocal images were grouped in two classes i.e., 1–8 min and 9–30 min post-agonist stimulation to monitor membrane and endosomal localization, respectively. The bar graphs indicate the % of cells showing βarr localization at the surface or in endosomal punctate structures in more than 500 cells for each condition collected from different field of views of three independent transfections and imaging experiments. Source data are provided as a Source Data file.

ability of Ib30 to recognize βarr1 in complex with several native GPCRs, although it was selected from a phage display library using V_2Rpp-βarr1 as the target[13,27]. Therefore, it would be worth probing the effect of Ib30 in the context of endocytosis and ERK1/2 phosphorylation for other receptors in future studies. Another interesting avenue where Ib30 may serve as a useful tool is the emerging paradigm of catalytic activation of βarrs, where they may continue to generate functional outputs even after dissociation from activated receptors[32–34]. It is plausible that Ib30 may recognize and stabilize such conformational "memory" in βarrs and thereby, facilitate its visualization in the cellular context as well as at high resolution using direct structural approaches.

In summary, we demonstrate that agonist-induced trafficking of βarrs and downstream responses can be allosterically modulated using conformation-specific intrabodies targeting protein-protein interactions. These findings open a paradigm for positively modulating GPCR signaling in cellular context and may catalyze the discovery of previously unknown aspects of GPCR-βarr interaction and functional outcomes.

Methods
General reagents
Most chemicals and molecular biology reagents were purchased from Sigma-Aldrich unless mentioned otherwise. HEK-293 cells (ATCC; cat. no. CRL-3216) were maintained at 37 °C under 5% CO_2 in Dulbecco's modified Eagle's medium (Gibco; cat. no. 12800-017) supplemented with 10% FBS (Gibco; cat. no. 10270-106) and 100 U ml⁻¹ penicillin and 100 µg ml⁻¹ streptomycin (Gibco; cat. no. 15140-122). Cells were cultured in 10 cm dishes (Corning; cat. no. 430167) at 37 °C under 5% CO_2 and passaged at 70 to 80% confluency using 0.05% trypsin-EDTA for detachment. *Sf*9 cells (Expression Systems; cat. no. 94-001 F) were maintained as suspension cultures in ESF 921 media (Expression Systems; cat. no. 96-001-01). Lauryl Maltose Neopentyl Glycol (LMNG) was purchased from Anatrace (cat. no. NG310).

Construct design and expression plasmids
The expression constructs for the wild-type human V_2R and V_2R^{T360A} mutants have been described previously[10]. Briefly, the cDNA coding for V_2R^{WT} with an N-terminal HA signal sequence and FLAG tag was PCR amplified and cloned in a customized pcDNA3.1 (+) vector. This construct was also cloned in pVL1393 vector for expression in *Sf*9 cells. The Thr360 mutation was generated on the V_2R^{WT} backbone using Q5 Site-Directed Mutagenesis Kit (NEB). The βarr1-mYFP plasmid used for confocal imaging experiments was obtained from Addgene (cat. no. 36916). βarr1-mCherry plasmid was a gift from Dr. Mark Scott, Institut Cochin, France. The plasmids encoding ScFv-CTL, ScFv30, Ib-CTL-HA, Ib30-HA and Ib30-YFP have been described previously[13,24]. The V_2R^{WT} and V_2R^{T360A} constructs were also fused with a 15 amino-acid flexible linker to the small subunit of NanoLuc i.e., SmBiT at its C-terminus. Similarly, Ib30 were N-terminally fused with LgBiT fragment in pCAGGS vector for NanoLuc complementation-based NanoBit assay. For in-vitro assays, i.e., trypsin proteolysis and ScFv30/Fab30 co-IP

experiments, βarr1 was purified from BL21 cells by Glutathione Sepharose (GS) affinity chromatography. All the constructs were sequence verified (Macrogen). V_2R agonist AVP (arginine-vasopressin) was synthesized by Genscript, and phospho-peptides V_2Rpp^{WT}, V_2Rpp^{T360-1}, and V_2Rpp^{T360-2} were synthesized by the peptide synthesis facility at Tufts University. The construct for GST-tagged β2-adaptin (residues 592–951, Rat, isoform 2) in pGEX4T1 vector was received as a kind gift from Dr. Thomas Pucadyil (Pune, India).

Limited trypsin proteolysis assay
To qualitatively assess the effect of different V_2R phospho-peptides i.e., V_2Rpp^{WT}, V_2Rpp^{T360-1} and V_2Rpp^{T360-2} on βarr1 conformation, limited trypsin proteolysis of βarr1 in the presence or absence of these phospho-peptides was performed. The protocol for trypsin proteolysis of βarr1 has been described previously[15]. Briefly, βarr1 (5–10 µM) was incubated in the absence or presence of (50:1 molar ratio, phospho-peptide: βarr1) the phospho-peptides for 30 min at 4 °C. Thereafter, L-1-Tosylamido-2-phenylethyl chloromethyl ketone (TPCK) treated Trypsin (Sigma-Aldrich; cat. no. T1426) was added to the βarr1 phospho-peptide mixture at a ratio of 1: 25 and 1: 50 (w/w) and the samples were incubated at 37 °C for 5 min. In addition to the indicated ratio of trypsin: βarr1, other ratios like 1: 10, 1: 100 and 1: 250 were also tried. At 1: 10 ratio, βarr1 was completely digested while at lower trypsin concentrations, the resolution of the digested fragments was poor. At each time point, 20 µl of the reaction mix (5 µg of βarr1) was withdrawn and transferred to a fresh microcentrifuge tube containing 5 µl of 5x SDS loading buffer to quench the proteolysis reaction. The digested samples were separated on 12% SDS-polyacrylamide gels by electrophoresis to determine the effect of phospho-peptides on the digestion pattern of βarr1. In addition, to study how ScFv30 affects the digestion pattern of βarr1 when activated with different phospho-peptides, a 50-fold molar excess of ScFv30 was added to the βarr1 samples prior to proteolysis. Samples without ScFv30 were used as references for comparison. After proteolysis with a 1: 50 ratio of trypsin: βarr1, the samples were quenched at 30 min and resolved by SDS-PAGE as described earlier.

Surface expression of receptor mutants
The surface expression of V_2R^{WT} and V_2R^{T360A} used in different cellular assays was measured by whole-cell surface ELISA. For this, HEK-293 cells transfected with either V_2R^{WT} or V_2R^{T360A} were seeded at a density of 0.2 million per well in a 24-well plate precoated with 0.01% poly-D-Lysine (Sigma-Aldrich; cat. no. P0899). After 24 h, cells were fixed with 4% (w/v) paraformaldehyde (pH 6.9) on ice for 20 min and washed three times with 1× tris-buffered saline (TBS) buffer [150 mM NaCl and 50 mM Tris-HCl (pH 7.4)]. Subsequently, nonspecific sites were blocked with 1% bovine serum albumin (BSA; prepared in 1× TBS) for 90 min, followed by the incubation of cells with horseradish peroxidase (HRP)-coupled anti-FLAG M2 antibody (dilution-1: 5000; Sigma-Aldrich; cat. no. A8592), prepared in 1% BSA for 90 min. Cells were then washed three times with 1% BSA in TBS, and 200 µl of
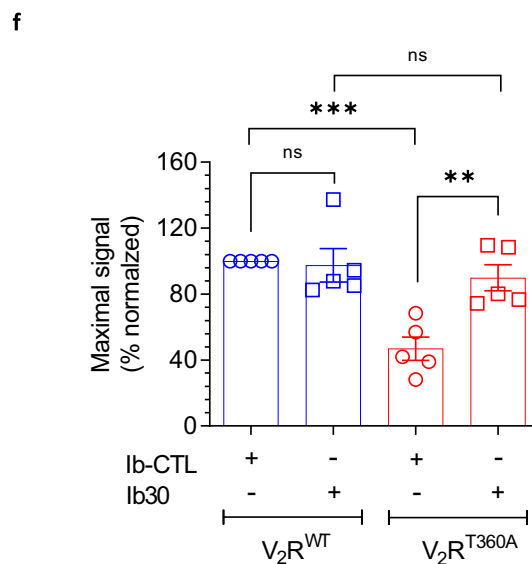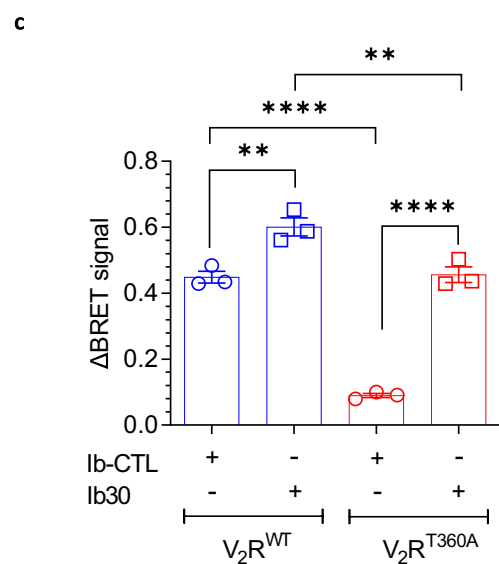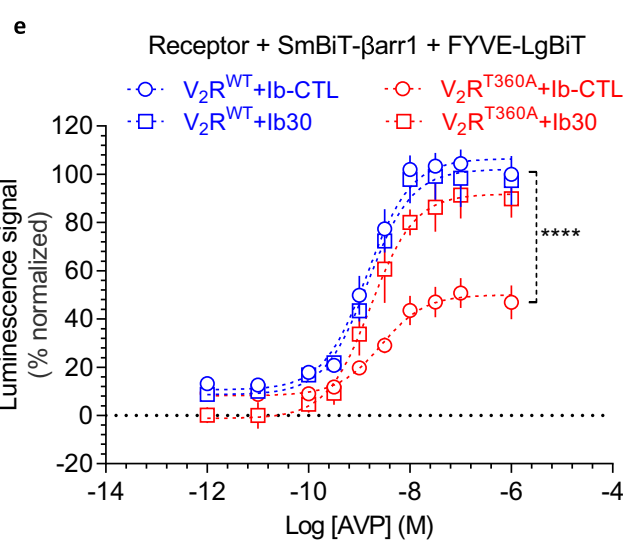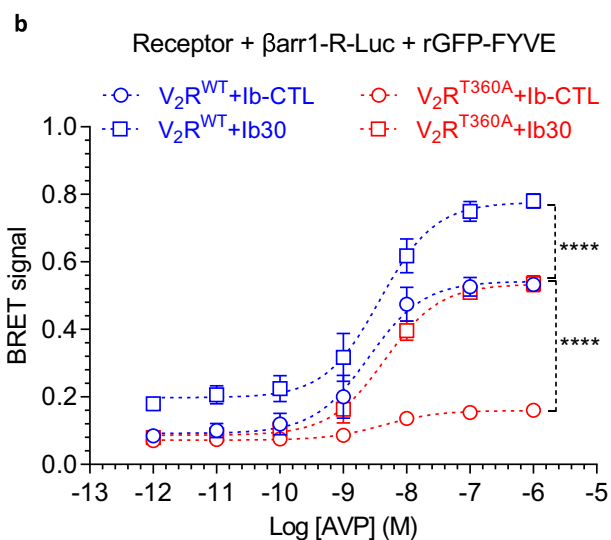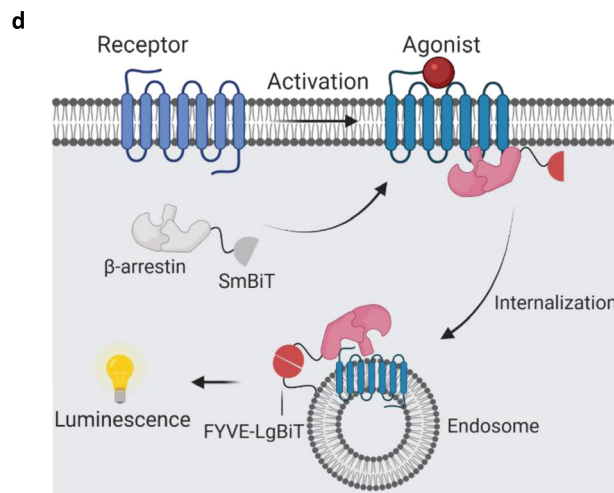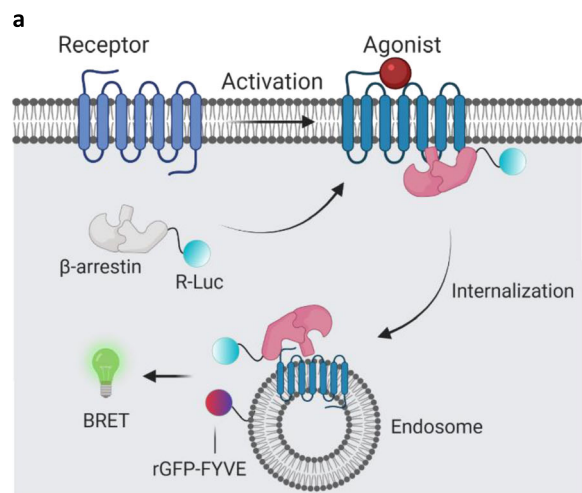
tetramethylbenzidine (TMB) ELISA substrate (Thermo Fisher Scientific; cat. no. 34028) was added to each well. Once blue color appeared in the wells, the reaction was stopped by transferring 100 μl of the solution to a different 96-well plate already containing 100 μl of 1 M H_2SO_4. Absorbance was measured at 450 nm in a multimode plate reader (Victor X4-Perkin-Elmer). For normalization of signal across different wells, cell density was estimated using Janus Green (Sigma-Aldrich; cat. no. 201677) staining. TMB solution was removed from the wells; cells were washed with 1× TBS followed by incubation with 0.2% (w/v) Janus Green for 20 min. Thereafter, cells were washed three times with distilled water and 800 μl of 0.5 N HCl was added to each well. 200 μl of this solution was used for measuring the absorbance at

Fig. 6 | Ib30 potentiates endosomal trafficking of βarr1 for the V_2R^{T360A} mutant. **a** Schematic representation of BRET-based endosomal localization assay for βarr1. **b** Co-expression of Ib30 promotes endosomal trafficking of βarr1 for V_2R^{T360A} as assessed by BRET assay. HEK-293 cells expressing the indicated constructs were stimulated with varying doses of AVP followed by BRET measurement. Data (mean ± SEM) from three independent experiments are presented here (Two-way ANOVA, Tukey's multiple comparisons test; ****$p < 0.0001$). **c** Comparison of ΔBRET (difference in the BRET signal at the lowest and highest dose of AVP) in the BRET assay based on the data presented in panel B from three independent experiments (mean ± SEM, One-way ANOVA, Tukey's multiple comparisons test; **$p < 0.01$, ****$p < 0.0001$). **d** Schematic representation of NanoBiT-based

endosomal localization assay for βarr1. **e** Co-expression of Ib30 robustly promotes endosomal trafficking of βarr1 for V_2R^{T360A} as assessed by NanoBiT assay. HEK-293 cells expressing the V_2R^{WT} or V_2R^{T360A}, together with SmBiT-tagged βarr1 and Ib-CTL/Ib30 were stimulated with indicated doses of AVP followed by luminescence measurement. Data (mean ± SEM) from five independent experiments, normalized with maximal response under V_2R^{WT} + Ib-CTL condition (treated as 100%) (Two-way ANOVA, Tukey's multiple comparisons test; ****$p < 0.0001$) are presented here. **f** Comparison of maximal response (at 1 μM AVP) in the NanoBiT-based endosomal trafficking assay presented in panel E from five independent experiments (mean ± SEM, One-way ANOVA, Tukey's multiple comparisons test; **$p < 0.01$, ***$p < 0.001$, ns = non-significant). Source data are provided as a Source Data file.
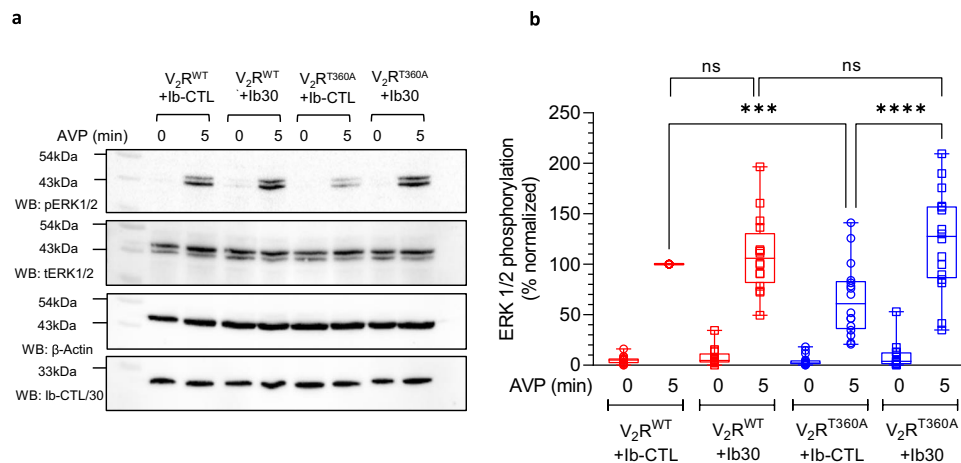
Fig. 7 | Ib30 potentiates agonist-induced ERK1/2 activation for the V_2R^{T360A} mutant. **a** HEK-293 cells expressing the indicated receptor construct together with Ib-CTL/Ib30 were stimulated with AVP (100 nM) followed by detection of ERK1/2 phosphorylation using western blot. The expression of Ib-CTL/Ib30 is monitored using anti-HA antibody. **b** Densitometry-based quantification from sixteen independent experiments, normalized with respect to V_2R^{WT} + Ib-CTL condition

(treated as 100%) (One-way ANOVA, Sidak's multiple comparisons test; ***$p = 0.0006$, ****$p < 0.0001$, ns = non-significant). The data represented as box plots showing median, IQR with whiskers of 1.5× IQR, and circles represent values from sixteen independent experimental replicates. Source data are provided as a Source Data file.

---

595 nm. Normalized surface expression of receptor constructs was calculated as the ratio of absorbance at 450 nm and 595 nm.

NanoBiT assay

NanoBiT assays were carried out following a previously published protocol[35]. Briefly, HEK-293 cells were transfected with the plasmids as indicated in the corresponding figures using PEI (Polyethylenimine; 1 mg ml^{-1}) as transfection agent at a DNA: PEI ratio of 1: 3. For total βarr1 recruitment (Fig. 4b), 4 μg of receptor-SmBiT and 3 μg of LgBiT-βarr1 were used, while for measuring surface recruitment (Fig. 4d), 3 μg of receptor, 2 μg of SmBiT-βarr1 and 5ug of LgBiT-CAAX were transfected. For the Ib30 reactivity assay (Fig. 5b), 5 μg of receptor, 5 μg of LgBiT-Ib30, and 2 μg of SmBiT-βarr1 were transfected. For endosomal trafficking experiment (Fig. 6e), 3 μg of receptor, 2 μg of SmBiT-βarr1, and 5 μg of FYVE-LgBiT were transfected. To measure the effect of Ib30 on total βarr1 recruitment (Supplementary Fig. 5b), 4 μg of receptor-SmBiT, 3 μg of LgBiT-βarr1 and either 6 μg of Ib-CTL or 1 μg of Ib30 were used. After 16–18 h of transfection, cells were harvested in PBS solution containing 0.5 mM EDTA and centrifuged. Cells were resuspended in 3 ml assay buffer (HBSS buffer with 0.01% BSA and 5 mM HEPES, pH 7.4) containing 10 μM coelenterazine (GoldBio; cat. no. CZ05) at final concentration. The cells were then seeded in a white, clear-bottom, 96-well plate at a density of 0.7–0.9 × 10^5 cells per 100 μl per well. The plate was kept at 37 °C for 90 min in the CO$_2$ incubator followed by incubation at room temperature for 30 min. Basal readings were taken in luminescence mode of a multi-plate reader (Victor X4-Perkin-Elmer). The cells were then stimulated with varying doses of ligand AVP ranging from 1 pM

to 1 μM (6x stock, 20 μl per well) prepared in drug buffer (HBSS buffer with 5 mM HEPES, pH 7.4). Luminescence was recorded for 60 min immediately after addition of ligand. The initial counts of 4–10 cycles were averaged and fold increase was calculated with respect to vehicle control (unstimulated values) and analyzed using nonlinear regression four-parameter sigmoidal concentration–response curve in GraphPad Prism software (v9.3).

Confocal microscopy

For visualizing the effect of intrabody on βarr-mediated receptor trafficking, HEK-293 cells were co-transfected with 3 μg of either V_2R^{WT} or V_2R^{T360A} along with 2 μg of βarr1-mYFP in the presence or absence of 2 μg of Ib30 with help of polyethylenimine (Polysciences; cat. no. 23966) reagent (21 μl) in 10 cm plates. Transfection was performed in FBS-deficient DMEM (Gibco; cat. no. 12800-017) after which cells were replaced with DMEM supplemented with FBS (Gibco; cat. no. 10270-106). Post 24 h, cells were seeded onto poly-D-lysine (Sigma-Aldrich; cat. no. P0899) precoated glass bottom confocal dishes (SPL Lifesciences; cat. no. 100350) at a density of 1 million per dish. Cells were allowed to adhere to confocal dishes for 24 h. The next day, cells were starved in FBS-deficient DMEM for 4 h and then stimulated with 100 nM AVP, and live cells were visualized under the confocal microscope (Zeiss LSM 710 NLO). The confocal microscope was equipped with a motorized XY stage along with a temperature and CO$_2$ controlled platform. For visualizing Ib30 and βarr1 together, cells were transfected with βarr1-mCherry (2 μg) and Ib30-mYFP (2 μg) along with V_2R^{T360A} (3 μg). To excite mYFP, a multi-line argon laser source was used and for the mCherry, a diode pump solid-state laser source was used.
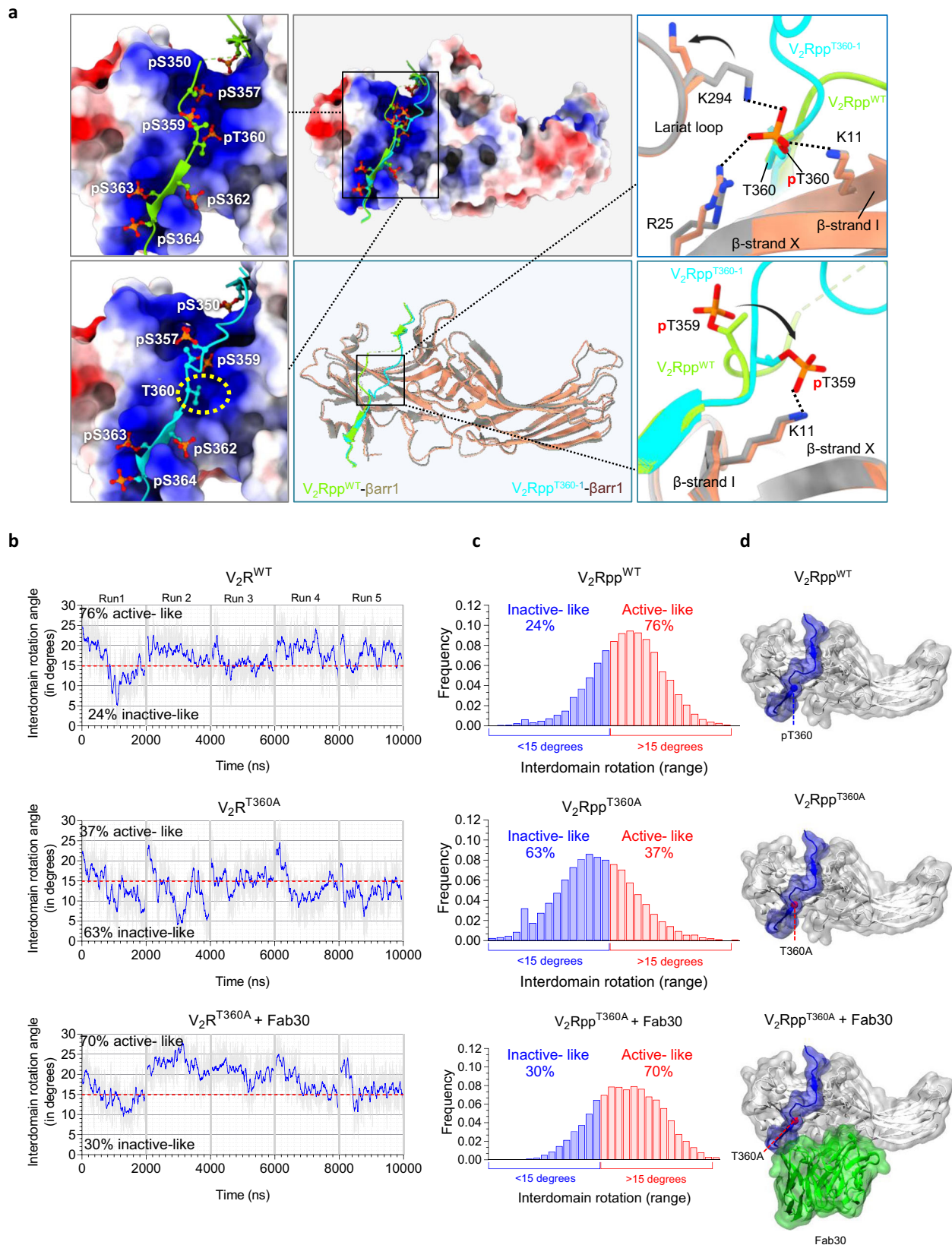
The emitted signal was detected with a 32× array GaAsP descanned detector (Zeiss). For related experiments, all microscopic settings including laser intensity and pinhole slit were kept in the same range and for avoiding any spectral overlap between two channels filter excitation regions and bandwidths were adjusted accordingly. Images were acquired in line scan mode and were subsequently processed post imaging in ZEN lite (ZEISS) software suite. For quantifying βarr trafficking to either membrane or endosomes, confocal images were categorized into early (1 to 8 min) and late time points (9 to 30 min) post agonist stimulation. The cells with βarr1-mYFP fluorescence in the plasma membrane were scored as surface localized, and the cells with punctate structures in the cytoplasm were scored as internalized. In

Fig. 8 | Intrabody30 (Ib30) stabilizes the active conformation of βarr1.
a Structural snapshots of βarr1 crystal structures in complex with V_2Rpp^{WT} (PDB: 4JQI) and V_2Rpp^{T360-1} (PDB: 7DFA). The superimposed structures display repositioning of the V_2Rpp^{T360-1} N-terminal segment harboring Thr^{360} residue (cyan) relative to the V_2R^{WT} (green). Also, changes in ionic interactions of Thr^{360} with neighboring residues are shown. For the V_2R^{WT} bound βarr1, Thr^{360} engages with Lys^{294}, Lys^{11}, and Arg^{25}. In the V_2R^{T360-1} bound state, the Thr^{360} is non-phosphorylated, and the side-chain of Thr^{359} is repositioned to interact with Lys^{11}. **b–d** MD

simulation of βarr1 in complex with either V_2Rpp^{WT} or V_2Rpp^{T360A} based on the crystal structure of V_2Rpp-βarr1 (PDB: 4JQI) reveals enrichment of inactive-like conformations of βarr1 in V_2Rpp^{T360A}-bound conformation. However, the binding of Fab30 to V_2Rpp^{T360A}-βarr1 complex robustly enriches the active-like conformational population of βarr1 as assessed by inter-domain rotation. The blue line in **8b** represents the rolling averages, while the grey line represents the original values for interdomain rotation per frame. Source data are provided as a Source Data file.

cases where βarrs were seen in both the membrane and in cytoplasmic punctate structures, cells having more than three punctae in the cytoplasm were scored under internalized category. Biological replicates were imaged at least three times independently on different days. Scored data from the cell count were plotted as the percentage of βarr recruitment from more than 500 cells for each condition. To avoid any discrepancies in manual counting, three different individuals counted the images in a blinded and cross-checked fashion. All data were plotted in GraphPad Prism software (v9.3).

Agonist-induced cAMP responses measured by GloSensor assay

To measure cAMP accumulation (as a readout for G protein activation), 50–60% confluent HEK-293 cells were co-transfected with either V_2R^{WT} or V_2R^{T360A} DNA (2 μg), luciferase-based 22 F cAMP biosensor construct (3.5 μg) and Ib-CTL (2 μg) or Ib30 (1 μg) DNA. After 18–20 h of transfection, cells were washed with 1xPBS and treated with trypsin-EDTA (0.05%). Detached cells were harvested and centrifuged at 184 X g for 10 min, and the cell pellet was resuspended in 0.5 mg ml⁻¹ luciferin (GoldBio; cat. no. LUCNA) solution prepared in 1X HBSS buffer (Gibco; cat. no. 14065) containing 20 mM HEPES (pH 7.4). Cells were then seeded at a density of 0.1–0.125 million per 100 μl in 96 well white plate. The same pool of cells was also seeded side by side for surface expression by whole cell surface ELISA. The cells seeded in 96-well plate were incubated for 1.5 h in 5% CO_2 followed by additional 30 min at room temperature. Subsequently, the basal luminescence was recorded for 5 cycles using a plate reader (Victor X4-Perkin-Elmer), followed by the addition of indicated concentrations of agonist AVP and luminescence was recorded for 1 h (30 cycles). Data were corrected for baseline signal and percent normalized with respect to maximal agonist concentration of V_2R^{WT} + Ib-CTL.

BRET assay for βarr1 trafficking

HEK-293T cells (ATCC) were grown in complete culture media (DMEM high glucose (Wisent; cat. no. 319-015-CL) supplemented with 10% FBS (Wisent; cat. no. 098150) and penicillin/streptomycin (Wisent; cat. no. 450-201-EL) in a tissue culture incubator set at 37 °C providing 5% CO_2. The day before transfection, cells were plated into well of a 6-well plate (Thermo scientific; cat. no. 140675) at 400,000 cells per well. The next day, media was changed for DMEM high glucose supplemented with only 2.5% FBS and cells were transfected using PEI (Polysciences; cat. no. 23966) as follows: 1 μg total DNA composed of 10 ng of V_2R^{WT} or V_2R^{T360A}, 25 ng of βarr1-RlucII, 100 ng of rGFP-FYVE and either 300 ng Ib-CTL or 50 ng Ib30 and DNA amount was completed with pcDNA3.1(+) was mixed with 3 μl of a 1 mg ml⁻¹ PEI solution and added drop-wise to cells. The plate was put back in the incubator till the next day. 24 h post-transfection, cells were detached and re-plated at 60,000 cells per well into a poly-L-ornithine-coated (Sigma-Aldrich; cat. no. P3655) white 96-well plate (Thermo scientific; cat. no. 236105) in complete culture media and left to grow for another 24 h. Then, the 96-well plate was washed once with Kreb's/HEPES solution (146 mM NaCl, 4.2 mM KCl, 0.5 mM $MgCl_2$, 1 mM $CaCl_2$, 5.9 mM glucose, and 10 mM HEPES buffer, pH 7.4) and 80 μl of Kreb's/HEPES was added per well. The plate was put back in the incubator for 2–3 h to allow cells to rest before BRET measurement. After the resting time, cells were stimulated for 15 min at 37 °C by adding 10 μl of AVP (Sigma-Aldrich; cat. no. V9879) at different concentrations prepared in Kreb's/HEPES. To

assess BRET, 10 μl of a 20 μM coelenterazine 400 A (GoldBio; cat. no. C-320) solution diluted in Krebs/HEPES was added 5 min before the end of the stimulation period. BRET was then monitored by measuring 3 consecutive luminescence readings at both 410 nm and 515 nm using a Tristar2 plate reader (Berthold. Technologies GmbH & Co. KG). BRET was calculated as the emission at 515 nm/emission at 410 nm and the 3 values were averaged. BRET data were plotted as dose-response curves using GraphPad Prism (v6).

Effect of Ib30 on agonist induced ERK1/2 phosphorylation

To assess the effect of Ib30 on βarr mediated signaling downstream to V_2R^{WT} and V_2R^{T360A} mutant, agonist-induced ERK1/2 phosphorylation was measured. For this, 60–70% confluent HEK-293 cells were co-transfected with 0.25 μg of indicated V_2R constructs and 1 μg of HA-tagged Ib30. A control intrabody (Ib-CTL) that does not recognize receptor-bound βarr1 was also transfected in parallel at levels comparable to Ib30 (3 μg) to achieve normalized expression levels of both the intrabodies. 24 h after transfection, cells were seeded into six-well plates at a density of 1 million cells per well. The next day, cells were serum-starved in DMEM for 6 h and were then stimulated with 100 nM AVP (agonist for V_2R) for indicated time points. After stimulation for selected time points, the media was aspirated and the cells were lysed in 100 μl of 2× SDS protein loading buffer. Cellular lysates were heated at 95 °C for 15 min, followed by centrifugation at 21130 X g for 15 min. 10 μl of samples were loaded per well and separated by 12% SDS-polyacrylamide gel electrophoresis. Phosphorylated ERK1/2 signal was detected by Western blotting using anti−phospho-ERK1/2 antibody (dilution-1: 5000; CST; cat. no. 9101) followed by reprobing of the blots with anti−total-ERK1/2 antibody (dilution-1: 5000; CST; cat. no. 9102). Since the anti−phospho-ERK1/2 and anti−total-ERK1/2 antibodies were not coupled to HRP, the Anti-Rabbit IgG-Peroxidase antibody (dilution-1: 5000; Sigma-Aldrich; cat. no. A9169) was used for signal detection. The expression of Intrabody was confirmed by probing with anti-HA antibody (dilution-1: 5000; Santa-Cruz; cat. no. sc-805). β-actin expression is used as a loading control (dilution-1: 50000; Sigma, Cat. no. A3854). Signal on the western blots was detected using the ChemiDoc imaging system (Bio-Rad), and densitometry-based quantification was carried out using ImageJ software suite.

Molecular dynamics simulations

Data without Fab30 was adapted from a previous study[10]. To generate V_2Rpp^{WT}-βarr1, V_2Rpp^{360A}-βarr1, and V_2R^{T360A}-βarr1-Fab30 complexes, we used previously determined crystal structure[27]. The sequence of βarr1 was reverted to match the isoform used in the in-vitro experiments [Uniprot AC: P29066]. The phosphorylation state of the V_2Rpp was retained from the used crystal structures. Missing fragments in the βarr1 and V_2Rpp structures were modeled using the loop modeller module available in the MOE package (www.chemcomp.com). In Fab30 we maintained residues 5 to 108 of the light chain and residues 1 to 123 of the heavy chain. The complexes were solvated (TIP3P water) and neutralized using a 0.15 concentration of NaCl ions. System parameters were obtained from the Charmm36M forcefield[36]. Simulations were carried out using the ACEMD3 engine[37]. Both systems underwent a 20 ns equilibration in conditions of constant pressure (NPT ensemble, pressure maintained with Berendsen barostat, 1.01325 bar pressure), using a timestep of 2 fs. During this stage
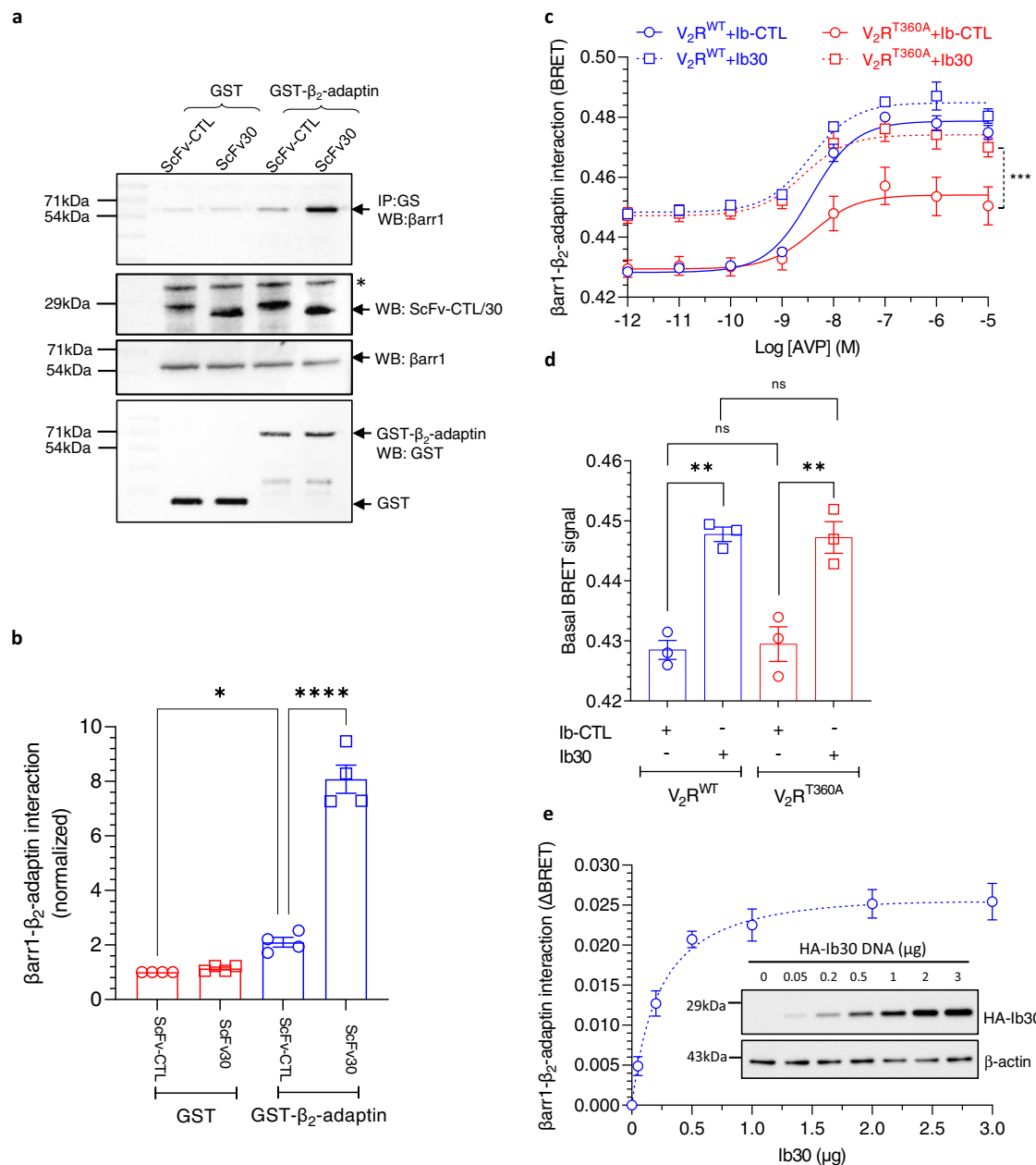
Fig. 9 | Intrabody30 enhances the interaction of β_2-adaptin with βarr1.
a Purified GST-β_2-adaptin (592–951) was incubated with V_2R^{T360A} and βarr1 in presence of ScFv-CTL or SvFv30 followed by co-IP and Western blotting. Unconjugated GST was used as a negative control. A representative blot from three different experiments is shown here. The * symbol designates a non-specific band that we typically observe in lysates prepared from *Sf*9 cells. **b** Densitometry-based quantification (mean ± SEM) of βarr1-β_2-adaptin interaction from four independent experiments normalized with GST control (One-way ANOVA, Sidak's multiple comparisons test; *p = 0.0308, ****p < 0.0001). **c** BRET between RlucII-tagged βarr1 and YFP-tagged β_2-adaptin shows enhanced interaction between βarr1 and β_2-adaptin in presence of Ib30, as compared to Ib-CTL, for both V_2R^{WT} and V_2R^{T360A}. Data (mean ± SEM) from three independent experiments (Two-way ANOVA,

Tukey's multiple comparisons test; ***p = 0.0006) are presented here. **d** The BRET signal at lowest ligand concentration under different conditions as measured in panel C from three independent experiments (mean ± SEM; One-way ANOVA, Tukey's multiple comparisons test; V_2R^{WT} (p = 0.0012); V_2R^{T360A} (p = 0.0020), ns = non-significant). **e** Ib30 induced increase in βarr1-β_2-adaptin interaction exists even in the absence of either V_2R^{WT} and V_2R^{T360A}. βarr1-β_2-adaptin interaction in presence of Ib30 exhibits a concentration-dependent increase until saturating concentration of the latter. Data represent four independent experiments (mean ± SEM). The *inset* shows a representative blot indicating the concentration range of Ib30 used in the BRET experiment, expression level and loading control (β-actin). Source data are provided as a Source Data file.

restraints were applied to the backbone. This was followed with 5×2 μs of simulation for each system in conditions of constant volume (NVT ensemble) using a timestep of 4 fs. This allowed us to amass a total of 10 μs simulation time per system. Simulations of inactive βarr1, as well as the V_2Rpp^{T360-1} βarr1 complex were carried out in a 3 x 500 ns setup. For each of the simulations we used a temperature of 310 K, which was maintained using the Langevin thermostat, hydrogen bonds were

restrained using the RATTLE algorithm. Non-bonded interactions were cut-off at a distance of 9 Å, with a smooth switching function applied at 7.5 Å. The inter-domain rotation angle of βarr1 was analysed using a script kindly provided by Naomi Latoracca[38]. The angle was measured by comparing the displacement of the C-domain relative to the N-domain between the inactive (PDB code: 1G4R) and active βarr1 crystal structures (PDB code: 4JQI). Each simulation frame was aligned

to the reference structures using the Cα atoms of the β-strands present within the N-domain, while the same atoms present in the C-domain were used to calculate the rotation angle. We have deposited all the simulation data presented in the current manuscript in the GPCRmd portal.

Co-immunoprecipitation (co-IP) assay

Co-IP was performed to evaluate the interaction between V_2Rpp^{WT}, V_2RppT^{360-1} and V_2Rpp^{T360-2} with βarr1 in presence of Fab30 and ScFv30. 5 μg of purified βarr1 was activated with 10-fold and 50-fold molar excess of phospho-peptides for 1 h at room temperature (25 °C) in binding buffer (20 mM HEPES, pH 7.4, 100 mM NaCl). Thereafter, the activated βarr1 was incubated with 2.5 μg of purified Fab30 or ScFv30. Subsequently, 20 μl of pre-equilibrated Protein L beads (GE Life-sciences; cat. no. 17547802) were added to the reaction mixture and incubated for an additional 1 h at room temperature, which was followed by extensive washing (3–5 times) with binding buffer + 0.01% LMNG. Elution was taken with 2X SDS loading buffer. Interaction of Fab30 and ScFv30 with βarr1 in presence of phospho-peptides was visualized using Coomassie staining of the gels. Band intensity was analysed by ImageJ gel analysis software.

To assess the effect of ScFv30 on V_2R^{T360A} induced βarr1-$β_2$-adaptin interaction, we performed co-immunoprecipitation assay (co-IP). The V_2R^{T360A} receptor was expressed in *Sf*9 cells, stimulated with 100 nM AVP and centrifuged to obtain receptor pellet. The receptor pellet was resuspended in appropriate volume of lysis buffer having 20 mM HEPES, 150 mM NaCl, 1X PhosSTOP (Roche; cat. no. 04906837001), and 1X protease inhibitor (Roche; cat. no. 04693116001), subjected to Dounce homogenization and incubated with 1 μg of purified βarr1 for 30 min at room temperature. The receptor-βarr complex was again incubated with 5 μg of purified ScFv30 or ScFv-CTL for another 30 min and solubilized with 1% LMNG for 1 h. Meanwhile, GST or GST-$β_2$-adaptin protein (2.5 μg) was immobilized on 20 μl buffer (20 mM HEPES, 150 mM NaCl) equilibrated GS beads (1 h at room temperature) and washed once to remove any unbound protein. Subsequently, the supernatant from solubilized complex was allowed to bind with protein bound GS beads (1 h at room temperature) followed by three washes with wash buffer (20 mM HEPES, 150 mM NaCl, 0.01% LMNG). The bead-bound complex was eluted in 2X SDS loading buffer. Eluted samples were separated by 12% SDS–polyacrylamide gel electrophoresis and probed using βarr antibody (dilution-1: 10000; CST; cat. no. 4674). After solubilization, 20 μl of lysate was set aside for confirming equal loading of βarr1 and ScFv. The lysate was run on separate 12% SDS–polyacrylamide gel and probed using βarr antibody and HRP-coupled protein L antibody (dilution-1: 2000; GenScript; cat. No. M00098) by western blotting. Band intensity was analysed by Image Lab software (Bio-Rad).

BRET assay for βarr1-$β_2$-adaptin interaction

To monitor βarr1 and $β_2$-adaptin interactions, BRET assays between βarr1-RlucII and $β_2$-adaptin-YFP were performed as described[22]. HEK-293 cells were seeded at a density of $1 × 10^6$ cells per 100 mm dish and transfected the next day with 250 ng of V_2R^{WT} or V_2R^{T360A} along with 120 ng of βarr1-RlucII, 1 μg of $β_2$-adaptin-YFP, and either 1.5 μg Ib-CTL or 1 μg Ib30 using PEI. Briefly, a total of 6 μg of DNA (adjusted with pcDNA3.1/zeo(+)) in 0.5 ml of PBS was mixed with 12 μl of PEI (25 kDa linear, 1 mg ml^{-1}) in 0.5 ml PBS and then incubated for 20 min prior to applying to the cells. After 24 h, cells were detached and seeded onto poly-ornithine-coated 96-well white plates at a density of ~35,000 cells per well for the BRET assays, which were performed 48 h after trans-fection. For BRET assays, cells in 96-well plates were washed once with Tyrode's buffer (140 mM NaCl, 2.7 mM KCl, 1 mM CaCl$_2$, 12 mM NaHCO$_3$, 5.6 mM D-glucose, 0.5 mM MgCl$_2$, 0.37 mM NaH$_2$PO$_4$, 25 mM HEPES, pH 7.4) and left in Tyrode's buffer for 1 h at room temperature. Cells were stimulated with various concentrations of AVP for 45 min

then BRET signals were measured using a plate reader (Victor X4-Perkin-Elmer). Coelenterazine h (Nanolight™, final concentration of 5 μM) was added 25 min prior to BRET measurement. The filter set used was 460/80 nm and 535/30 nm for detecting the RlucII, *Renilla* luci-ferase (donor) and YFP (acceptor) light emissions, respectively. The BRET ratio was determined by calculating the ratio of light emitted by YFP over light emitted by RlucII. For Ib30 titration, HEK-293 cells were transfected with 120 ng of βarr1-RlucII and 1 μg of $β_2$-adaptin-YFP along with various amounts (0 to 3 μg) of Ib30 in 100 mm dishes or scaled down to 1/6 in a well in 6well plates. BRET signals were measured in absence of ligand stimulation. Expression levels of Ib30 were accessed by western blotting with anti-HA-peroxidase conjugate (dilution-1: 1000, Sigma-Aldrich; cat. no. 12013819001). Anti-β-actin antibody (dilution-1: 2000, Santa Cruz Biotechnology; cat. no. sc-47778) was used for loading control.

Data quantification and statistical analysis

The experiments were conducted at least three times and data (mean ± SEM) were plotted and analyzed using GraphPad Prism soft-ware (v9.3). The data were normalized with respect to proper experi-mental controls and appropriate statistical analyses were performed as indicated in the corresponding figure legends.

Reporting summary

Further information on research design is available in the Nature Research Reporting Summary linked to this article.

Data availability

The original raw data for gels, immunoblots and confocal micrographs have been deposited in Mendeley Data (https://doi.org/10.17632/8wmkcw8ht7.1). This paper does not report any original code. The coordinates for V_2Rpp^{WT}-βarr1 and V_2Rpp^{T360-1}-βarr1 crystal structures used in this study are available in PDB with ID 4JQI and 7DFA, respec-tively. Any additional information required to reanalyze the data reported in this paper is available from the corresponding author upon reasonable request. Source data are provided with this paper. Original data pertaining to MD simulation are deposited in GPCRmd (https://submission.gpcrmd.org/dynadb/publications/1486/). Source data are provided with this paper.

References

1. Bockaert, J. & Pin, J. P. Molecular tinkering of G protein-coupled receptors: an evolutionary success. *EMBO J* **18**, 1723–1729 (1999).
2. Pierce, K. L., Premont, R. T. & Lefkowitz, R. J. Seven-transmembrane receptors. *Nat. Rev. Mol. Cell Biol.* **3**, 639–650 (2002).
3. Hauser, A. S., Attwood, M. M., Rask-Andersen, M., Schioth, H. B. & Gloriam, D. E. Trends in GPCR drug discovery: new agents, targets and indications. *Nat. Rev. Drug Discov.* **16**, 829–842 (2017).
4. Lefkowitz, R. J. & Shenoy, S. K. Transduction of receptor signals by beta-arrestins. *Science* **308**, 512–517 (2005).
5. Kang, D. S., Tian, X. & Benovic, J. L. Role of beta-arrestins and arrestin domain-containing proteins in G protein-coupled receptor trafficking. *Curr. Opin. Cell Biol.* **27**, 63–71 (2014).
6. Ranjan, R., Dwivedi, H., Baidya, M., Kumar, M. & Shukla, A. K. Novel structural insights into GPCR-beta-arrestin interaction and signal-ing. *Trends Cell Biol.* **27**, 851–862 (2017).
7. Gurevich, V. V. & Gurevich, E. V. The molecular acrobatics of arrestin activation. *Trends Pharmacol. Sci.* **25**, 105–111 (2004).
8. Oakley, R. H., Laporte, S. A., Holt, J. A., Caron, M. G. & Barak, L. S. Differential affinities of visual arrestin, beta arrestin1, and beta arrestin2 for G protein-coupled receptors delineate two major classes of receptors. *J. Biol. Chem.* **275**, 17201–17210 (2000).
9. Nobles, K. N. et al. Distinct phosphorylation sites on the beta(2)-adrenergic receptor establish a barcode that encodes differential functions of beta-arrestin. *Sci. Signal* **4**, ra51 (2011).

10. Dwivedi-Agnihotri H., et al. Distinct phosphorylation sites in a prototypical GPCR differently orchestrate beta-arrestin interaction, trafficking, and signaling. *Sci. Adv.* **6**, eabb8368 (2020).

11. Baidya, M. et al. Key phosphorylation sites in GPCRs orchestrate the contribution of beta-Arrestin 1 in ERK1/2 activation. *EMBO Rep.* **21**, e49886 (2020).

12. Chen, J. et al. Individual phosphorylation sites at the C-terminus of the apelin receptor play different roles in signal transduction. *Redox Biol.* **36**, 101629 (2020).

13. Baidya, M. et al. Genetically encoded intrabody sensors report the interaction and trafficking of beta-arrestin 1 upon activation of G-protein-coupled receptors. *J. Biol. Chem.* **295**, 10153–10167 (2020).

14. Xiao, K., Shenoy, S. K., Nobles, K. & Lefkowitz, R. J. Activation-dependent conformational changes in {beta}-arrestin 2. *J. Biol. Chem.* **279**, 55744–55753 (2004).

15. Nobles, K. N., Guan, Z., Xiao, K., Oas, T. G. & Lefkowitz, R. J. The active conformation of beta-arrestin1: direct evidence for the phosphate sensor in the N-domain and conformational differences in the active states of beta-arrestins1 and −2. *J. Biol. Chem.* **282**, 21370–21381 (2007).

16. Ghosh, E. et al. Conformational Sensors and Domain Swapping Reveal Structural and Functional Differences between beta-Arrestin Isoforms. *Cell Rep.* **28**, 3287–3299 e3286 (2019).

17. Winn, M. D. et al. Overview of the CCP4 suite and current developments. *Acta Crystallogr. D. Biol. Crystallogr.* **67**, 235–242 (2011).

18. Namkung, Y. et al. Monitoring G protein-coupled receptor and beta-arrestin trafficking in live cells using enhanced bystander BRET. *Nat. Commun.* **7**, 12178 (2016).

19. Shenoy, S. K. et al. Ubiquitination of beta-arrestin links seven-transmembrane receptor endocytosis and ERK activation. *J. Biol. Chem.* **282**, 29549–29562 (2007).

20. Laporte, S. A. et al. The beta2-adrenergic receptor/betaarrestin complex recruits the clathrin adaptor AP-2 during endocytosis. *Proc. Natl Acad. Sci. USA* **96**, 3712–3717 (1999).

21. Laporte, S. A., Miller, W. E., Kim, K. M. & Caron, M. G. beta-Arrestin/AP-2 interaction in G protein-coupled receptor internalization: identification of a beta-arrestin binging site in beta 2-adaptin. *J. Biol. Chem.* **277**, 9247–9254 (2002).

22. Beautrait, A. et al. A new inhibitor of the beta-arrestin/AP2 endocytic complex reveals interplay between GPCR internalization and signalling. *Nat. Commun.* **8**, 15054 (2017).

23. Irannejad, R. et al. Conformational biosensors reveal GPCR signalling from endosomes. *Nature* **495**, 534–538 (2013).

24. Ghosh, E. et al. A synthetic intrabody-based selective and generic inhibitor of GPCR endocytosis. *Nat. Nanotechnol.* **12**, 1190–1198 (2017).

25. Gulati, S. et al. Targeting G protein-coupled receptor signaling at the G protein level with a selective nanobody inhibitor. *Nat. Commun.* **9**, 1996 (2018).

26. He, Q. T. et al. Structural studies of phosphorylation-dependent interactions between the V2R receptor and arrestin-2. *Nat. Commun.* **12**, 2396 (2021).

27. Shukla, A. K. et al. Structure of active beta-arrestin-1 bound to a G-protein-coupled receptor phosphopeptide. *Nature* **497**, 137–141 (2013).

28. Kumari, P. et al. Core engagement with beta-arrestin is dispensable for agonist-induced vasopressin receptor endocytosis and ERK activation. *Mol. Biol. Cell* **28**, 1003–1010 (2017).

29. Kumari, P. et al. Functional competence of a partially engaged GPCR-beta-arrestin complex. *Nat. Commun.* **7**, 13416 (2016).

30. Cahill, T. J. 3rd et al. Distinct conformations of GPCR-beta-arrestin complexes mediate desensitization, signaling, and endocytosis. *Proc. Natl Acad. Sci. USA* **114**, 2562–2567 (2017).

31. Shiraishi Y., et al. Biphasic activation of beta-arrestin 1 upon interaction with a GPCR revealed by methyl-TROSY NMR. *Nat. Commun.* **12**, 7158 (2021).

32. Eichel, K. et al. Catalytic activation of beta-arrestin by GPCRs. *Nature* **557**, 381–386 (2018).

33. Eichel, K., Jullie, D. & von Zastrow, M. beta-Arrestin drives MAP kinase signalling from clathrin-coated structures after GPCR dissociation. *Nat. Cell Biol.* **18**, 303–310 (2016).

34. Ranjan, R., Gupta, P. & Shukla, A. K. GPCR signaling: beta-arrestins Kiss and Remember. *Curr. Biol.* **26**, R285–R288 (2016).

35. Dwivedi-Agnihotri, H. S. P., Deeksha, S., Kawakami, K., Inoue, A. & Shukla, A. K. An intrabody sensor to monitor conformational activation of β-arrestins. *Methods Cell Biol.* **169**, 267–278 (2022).

36. Huang, J. et al. CHARMM36m: an improved force field for folded and intrinsically disordered proteins. *Nat. Methods* **14**, 71–73 (2017).

37. Harvey, M. J., Giupponi, G. & Fabritiis, G. D. ACEMD: accelerating biomolecular dynamics in the microsecond time scale. *J. Chem. Theory Comput.* **5**, 1632–1639 (2009).

38. Latorraca, N. R. et al. Molecular mechanism of GPCR-mediated arrestin activation. *Nature* **557**, 452–456 (2018).

Acknowledgements

Author contributions

M.B. (MBA) carried out confocal microscopy, assisted in the NanoBiT assay, β2-adaptin interaction experiments using co-immunoprecipitation and ERK1/2 MAP kinase activation experiments; M.C. generated the receptor constructs with the help from P.S., carried out the limited proteolysis experiment with A.R., participated in β2-adaptin interaction experiments using co-IP, and performed ERK1/2 MAP kinase activation experiments with S.P.; HD-A carried out GloSensor assay with the help from M.C. and NanoBiT assay with MBA and PS, participated in β2-adaptin interaction experiments using co-IP; M.B. (MB), B.P., and M.K.Y. performed Fab30/ScFv30 co-IP assay; R.B. and J.M. carried out structural analysis of crystal structures; D.D. performed BRET experiments to monitor endosomal trafficking of βarr1 under the

Competing interests

Additional information